VUF-1013
FINAL REPORT

VELA UNIFORM

PROJECT SHOAL

SPONSORED BY THE ADVANCED RESEARCH PROJECTS AGENCY OF THE DEPARTMENT OF DEFENSE AND THE U.S. ATOMIC ENERGY COMMISSION

FALLON, NEVADA
OCTOBER 26, 1963

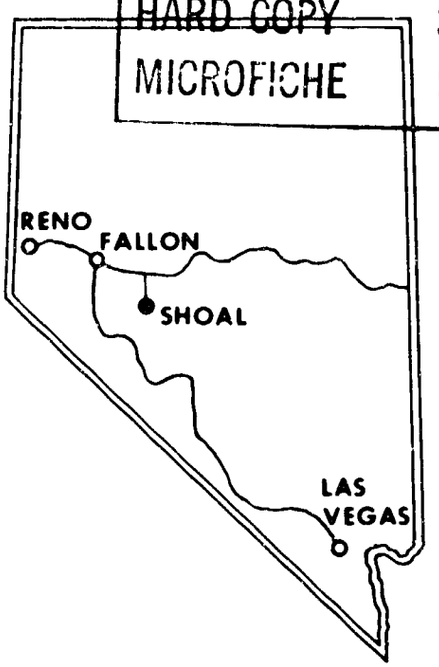

ANALYSIS OF SHOAL DATA ON GROUND MOTION AND CONTAINMENT

Roland F. Beers, Inc.

December 4, 1964

Issuance Date: January 11, 1965

LEGAL NOTICE

NUCLEAR EXPLOSIONS—PEACEFUL APPLICATIONS
TID-4500(37th Ed.)

PROJECT SHOAL

Final Report

ANALYSIS OF SHOAL DATA ON GROUND MOTION AND CONTAINMENT

SAFETY PROGRAM

December 4, 1964

Roland F. Beers, Inc.
Alexandria, Virginia

CONTENTS

CONTENTS (continued)

CONTENTS (continued)

ABSTRACT

Predictions and evaluations of ground motion and containment were made for the 12.5 kt Shoal event. A comprehensive ground motion instrumentation program was designed. This program included four linear instrument arrays radiating northeast, northwest, southeast and southwest with a total of 21 stations. Eight additional stations were emplaced at points of interest. Of the 29 stations, 21 were on hardrock and eight were on alluvium.

Analysis of the seismic records included corrections for instrument response and derivation of non-recorded motions by differentiation or integration. It was determined that peak motions on alluvium were greater than on hardrock by a factor of 2.1 for acceleration, 3.7 for displacement and 3.4 for velocity. The rates of attenuation indicated that peak motions on alluvium were not due to surface waves. The prediction equations for acceleration and displacement were found to represent reasonable upper limits of motion.

The objective of the containment evaluation was to assure that appropriate measures had been taken to preclude unacceptable venting of radioactive isotope to the

atmosphere. Consideration was given to possible venting both at the time of the explosion and later when the cavity collapsed and a chimney formed. The adequacy of stemming of all man-made openings as well as the effect of geologic hazards such as faults or fissures were evaluated in the containment analysis. The possibility of a secondary explosion due to water entering the cavity was also examined. It was concluded that Shoal would be contained to the same degree as Hardhat and that the stemming plan was adequate.

The prediction of containment was substantiated by the test results. Limited post-shot exploration allows the following comparisons: cavity radius - 24.7 meters predicted, 25.6 $\pm$ 0.6 meters observed; chimney height - 110 meters predicted, 108 meters observed; depth of spalling - 122 meters predicted, 120+ meters indicated; radius of spalling - <914 meters predicted, 794 meters observed.

CHAPTER I

INTRODUCTION

1.1 BACKGROUND

Roland F. Beers, Inc., under Contract AT(29-2)-1163 with the Nevada Operations Office (NVOO), U. S. Atomic Energy Commission (AEC) is responsible to the Operational Safety Division of that office for the following:

a) Prediction of ground motions

b) Evaluation of containment of underground nuclear explosions

The 12.5 kt Shoal event was the second, and largest, contained underground nuclear test conducted in granite. This event presented special prediction problems due to the absence of directly applicable experience and its location off the Nevada Test Site in the Sand Springs mountain range near Fallon, Nevada.

Ground motion resulting from underground testing of nuclear devices is a substantial as well as continuing operational safety problem. Current methods of predicting ground motion employ empirical relationships derived from observed data. Proper use of these relationships for prediction purposes requires that the test conditions

for which predictions are to be made be comparable with those which provided the data used in deriving the relationships.

Scaling of ground motion for yield and distance are fundamental steps in making predictions. To perform such scaling, the variation in amplitude with yield and distance must be defined. Appreciable departure in yield, source geometry, method of emplacement and physical properties of the transmission path from previous experiments substantially affect manner of scaling and the agreement between predicted and observed ground motions.

The results of the earlier 5.9 kt Hardhat event in granite on NTS were not used. The limited span of distances at which ground motion data were recorded from Hardhat and the high degree of scatter in surface-recorded data resulted in an ambiguous rate of attenuation of ground motion with distance. Additionally, as Hardhat was the only test conducted in granite prior to Shoal, the empirical scaling of amplitude with yield was indeterminate. To find an alternate basis for making predictions, the displacement potentials were compared for the different media in which tests have been conducted to date. This

comparison suggested that potentially more accurate results, especially at larger distances, should be obtained using tuff as a basis for predicting ground motions. Accordingly, prediction relationships were derived from the results of the Hardtack-Plumbob experiments in Rainier Mesa tuff. However, differences between the geology of the Shoal site and Rainier Mesa introduced substantial uncertainty. The scope of the transmission problem is defined in Section 1.4.

The possibility of a containment failure is a recurring problem. This hazard becomes particularly important when an off-site event is considered. In analyzing the Shoal event from this viewpoint, the Hardhat event provided the only previous experience in a granitic medium upon which to base predictions. The prediction of phenomenology, therefore, relied heavily upon the available Hardhat data. Where conditions were dissimilar, theoretical analysis and extrapolation of experience from other media were employed. These techniques permitted an evaluation to be made of unique conditions such as the stemming design and the presence of a significant fault in the vicinity of the weapon point.

1.2 OBJECTIVES

In regard to containment, the purpose was to provide the Operational Safety Division with an independent evaluation of the probability of containment and the adequacy of the stemming concept and plan. In performing this function, dependence was placed on theoretical considerations and on empirical data collected in large measure by others. This supply of data was arranged primarily by the NVOO, but also was obtained by direct contact with the Technical Director where appropriate.

To evaluate the effect of the varied geology on ground motion, a comprehensive ground motion measurement program was designed. Instrumentation program design objectives for the Shoal event were to obtain ground motion data permitting evaluation of the following:

1) The variation in the amplitude of ground motions on granite and alluvium with distance.
2) The effect of faulting on ground motion.
3) The effect of thickness of alluvium on the amplitude and attenuation of amplitude with distance.
4) The partition of compressional wave energy into surface waves at a lithologic discontinuity.

5) The directional response characteristics of the shot medium.

6) The degree of scatter in recorded ground motions.

7) The ratio of (u^2/ad) where "u" is particle velocity, "a" is particle acceleration, and "d" is particle displacement.

1.3 INSTRUMENTATION

To accomplish the objectives listed in Section 1.2, 21 recording stations were deployed in four linear arrays radiating northeast, northwest, southeast and southwest from ground zero (see Figure 1.1). Each of these 21 stations had an instrument complement of three component accelerometers and three component displacement meters. Three of the 21 recording stations also included instruments for recording three components of velocity. These instruments were located on the southeast line. Besides the above, vertical component velocity measurements were made at five additional stations at distance. Each of the vertical component measurements represents the output of a circular array of six vertical velocity instruments emplaced at widely separated points surrounding the test site. An additional

three vibration meters measuring radial and transverse displacement were located at the Nevada Scheelite Mine, Gabbs Mine and the Naval Air Station.

Of the 21 recording stations deployed in arrays, fourteen were located on granite and seven were located on alluvium. To evaluate the transmission properties of granite, the positions of the recording arrays located on granite were given preferential azimuthal orientations related to the more predominant NE-SW system of faulting. The arrays oriented northeast-southwest essentially parallel this system of faulting while the arrays oriented northwest-southeast intersect this faulting essentially at right angles. Evaluation of the effect of different lithology was provided for by extending the arrays from granite to alluvium. Evaluation of the effect of different thicknesses of alluvium was provided for by locating one of the arrays on the thick alluvium of Fairview Valley and the other on the thinner alluvium of Fourmile and Eightmile Flats. The circular arrays of vertical component velocity meters emplaced at distance were on hardrock of unknown lithology. These were not part of the safety studies program. The vibration meters were emplaced to monitor ground motions at sites of engineering structures.

1.4 THEORY

1.4.1 Seismic Effects. At the Shoal site considerable variation in the amplitudes of the particle motions was expected to occur both horizontally and directionally due to asymmetries in the geometry and geology of the transmission model. Figure 1.2 is a cross section showing the attitudes of the granite-alluvium contact on either side of the site. The eastern contact of the granite with the alluvium is abrupt with nearly vertical dip and with a great depth of alluvium directlv adjacent to the granite. The western edge of the granite shows much less dip with alluvium forming a wedge over the granite.

The geologic map of Figure 1.3 shows the trend of faulting at the Shoal site as far as it is known. The major trend is northeast-southwest on the basis of surface evidence but it should be noted that a major fault trending east-west lies at a radial distance of approximately 34 meters north of the working point. The multiplicity of southeast-northwest trending features indicated on the map are dikes.

The Shoal model described above departs from the homogeneous, isotropic conditions usually assumed. The many

faults, joints and dikes in the granite were expected to have an effect on azimuthal variation of ground motion. The energy transmission parallel to the northeast-southwest set would be enhanced as compared to energy transmission at right angles to the fault set. This means that energy reaching the alluvium of Fourmile Flat and Fairview Valley at the points closest to the working point may be less than that normally expected. The energy along the Sand Springs Range would be about as expected to the south and slightly lower than expected to the north due to the large east-west fault just north of the working point.

The second aspect of the model relates to the presence of the alluvium in the adjacent Fourmile Flat and Fairview Valley areas. The question here was whether surface waves generated at the contact between granite and alluvium would produce larger ground motions at distances on the alluvium than those resulting from compressional (body) wave arrivals. The amplitude of the ground motion due to surface waves for a two-media model depends on diverse factors. Some of these are: the distance of the granite-alluvium contact from the source, the dip of the contact, the partition of energy from compressional waves into surface waves, and the thickness of alluvium at the contact

and along the transmission path to the point of interest. Although Ewing, Jardetzky and Press (Reference 19) have developed surface wave theory for specialized cases, there was no known theory applicable to the Shoal model. Together with this, there was also a lack of empirical data on partition of energy from compressional into surface waves.

On the other hand, to predict the ground motions at the surface of the alluvium due to compressional waves, it is required to increase the amplitudes of predicted free-field particle motions by some factor. This factor probably depends on the interrelationship of wave period to bed thickness. The factor two has been commonly used in the past to convert from surface to subsurface motion, but this does not include effects of transmission from one rock type to another. Because of these uncertainties, no factor was applied in making predictions of Shoal seismic effects on alluvium.

1.4.2 Phenomenology and Containment. The evaluation of containment of the Shoal event was based on procedures developed as part of a long range program directed to the continuing improvement of confidence in predictions.

Currently, greater dependence is placed on empirical relationships, and it is probable that experience will always be a major factor in evaluation. However, a large part of the improvement will come from greater knowledge of the pressure-time history and temperature-time history of underground explosions. This is being actively pursued, and some of the results were employed in the development of predictions and the evaluation for Shoal.

CHAPTER II

PREDICTIONS

2.1 GEOLOGIC ENVIRONMENT

The local geologic and topographic setting of the Sand Springs Range and the surrounding terrain has been amply provided by the text, maps and cross sections of Reference 1. A cross section and a portion of a map from this reference are included in Chapter 1.

The lithology of the granitic shot medium is also described in Reference 1. Its physical properties have been compiled from several sources and are tabulated in Table 2.1.

The significant structural features of the region include a well-developed fracture cleavage which persists throughout the granitic medium. Generally, planes are .25 to .51 cm apart, trending northeast, with a near vertical dip. Also, steeply dipping well-developed joints trend northwesterly (Reference 1).

The entire Sand Springs Range is heavily faulted, the strongest trend being northeasterly. However, geologic evidence from ECH-D (Reference 1), the east drift (Reference 2), and test holes B-1 through B-4, (References 3 and 4) indicate with certainty that no significant faults exist within a 30 meter radius of the Working Point (W.P.). The test holes indicate that the

nearest fault is the so-called Fault E which, prior to detonation, lay at a radial distance of about 34 meters from the W.P. Correlation with its probable surface exposure indicates that the fault strikes approximately east-west and dips 70 degrees south. Its true pre-shot thickness, where intersected by ECH-D, was about 34 meters.

Because of considerable core loss in drilling ECH-D in the fault zone, the material character was not directly observed. However, geophysical logs of this hole suggest the zone is composed of slightly-to-completely decomposed granite containing water, most of which is fixed molecularly by hydration of feldspar. Large voids are probably absent and the fault material is considered to be mostly impervious.

The next nearest known fault is Zone C, originally identified on the surface and later intersected by the east drift at Station 8 + 42. It strikes approximately north - 22 degrees - east and dips about 74 degrees southeast. Its true thickness is about 3.65 meters, and is composed chiefly of slickensided gouge (Reference 2).

Ground water within the granite occurs within joints, fractures and faults which are probably incompletely connected and which may or may not share a vague and irregular water table. Initially, such a surface was found at a

depth of about 294 meters in Hole ECH-D (Reference 1). A later pump test prior to underground excavation indicated the water level may have dropped to a depth of 316 meters. It seems likely that many of the local water-bearing zones have been lowered appreciably as a result of drainage by subsequent underground excavation. Nonetheless, the continued heavy flow from Hole E-1 (Reference 5) indicated that considerable ground water with appreciable head remained in the vicinity at the shot time. Furthermore, the discontinuous nature of the ground water indicates that a water-bearing zone could remain essentially unchanged by drift excavation and could retain its initial hydrostatic head. Therefore, as stated in Reference 6, it is conceivable that such a water-bearing zone exists within the fracture limit of the detonation.

2.2 PHENOMENOLOGY AND CONTAINMENT

The following sections provide the basis for the predictions shown in the abstract pertaining to close-in phenomena and containment problems.

2.2.1 Radius of Cavity. The predicted cavity radius was 24.7 meters. This was based on cube-root scaling from Hardhat where the observed cavity radius was 19.2 meters (Reference 7). The yield used for Shoal was the measured 12.5 kt and that for Hardhat was

5.9 kt. The chamber sizes for Hardhat and Shoal are comparable. Accordingly, cube-root scaling should be applicable. A check was performed establishing the peak pressure at the cavity radius for Hardhat and computing the distance for equal pressure for Shoal. This confirmed the cube-root scaling procedure.

2.2.2 Cracking Radius. Radial cracking for the Shoal event was predicted to extend to approximately 159 meters in the free field and possibly greater distances where the presence of openings produces a free-face effect.

The extent to which fractures will be propagated due to a subsurface detonation has been found to depend upon the physical properties of the shot medium. It is therefore necessary to rely upon past experience in the medium and any experimental data which have a bearing on the problem. From Hardhat it was found that post-shot fractures, observable in the tunnel, extended to a distance of 159 meters from the W.P. (Reference 8); free-field fractures would be expected to be less but no maximum value is recorded for these. Radioactivity was encountered in the end of the Hardhat drift and therefore continuous channels for transport must have existed out to this distance, a radius of approximately 61 meters. This may then constitute a minimum free-field fracture radius.

The above values were used to predict the extent of radial fracturing anticipated for the Shoal event by considering the permanent radial displacements and associated strains for the two events. The predicted and observed radial displacements were derived by a method similar to that outlined in Appendix A and are shown in Figures 2.1 and 2.2. The use of strain data in obtaining predictions of fracturing radius is logical if the mode of deformation is considered. As the cavity expands, the forces existing in the free field are a radial compression coupled with a tangential expansion. This situation may be approximated by uniaxial compression tests since the stresses created by tangential tension cannot become large for geologic materials. The permanent strain of 159 meters for Hardhat was 0.125 percent as obtained from Figure 2.1. Using this strain, fracturing would extend to a distance of 201 meters for Shoal. Similarly, a minimum value was established for Shoal by considering the strain at 61 meters for Hardhat since radioactive contamination entered the drift at this radius. This yielded a radial distance of about 76 meters for an equivalent strain at Shoal.

Since the maximum fracturing radius observed in tunnels is certainly greater than in the free-field condition, it is necessary to obtain estimates of the latter.

From results of three uniaxial compression tests on

the Shoal granite cores by the Waterways Experiment Station, an average maximum compressive strain of 0.25 percent was indicated (Reference 9). This strain corresponds to that predicted at 159 meters for the Shoal event.

Additionally, an examination of uniaxial compressive tests on Unaweep granite cores (Reference 10) revealed that a strain of 0.33 percent was sufficient to produce fracturing. Utilizing this strain, a free-field fracture radius of 146 meters was predicted for the Shoal event. These predictions appeared reasonable in the light of maximum and minimum figures previously established and the fact that fracture strains for various granites vary only slightly. A radius of 159 meters was therefore predicted as the outer limit of free-field fracturing.

2.2.3 Radius of Radiation Injection into Cracks by Particulates and Condensates. Data concerning the radial distribution of radioactive materials in fractures are very limited. The outer limit of radioactivity indicated at Rainier was about 58 meters (Reference 11). The outer limit of fracturing shown in Table 14 (Reference 12) was 85.3 meters. Assuming that the ratio of the radius of radioactivity to the radius of cracking is constant for various media, then the outer limit of radioactivity for Shoal would have been

$$(58/85.3) \times 159 \text{ meters} = 108 \text{ meters}$$

where 159 meters is the cracking radius as predicted in Section 2.2.2. A check was made by considering that radioactivity entered the Hardhat drift at a distance of at least 61 meters. By a computation similar to that outlined in Section 2.2.2 a minimum radioactive fracture radius for Shoal was found to be about 91.4 meters.

2.2.4 Height of Chimney. A chimney height of 110 meters was predicted. This was based on the calculation described in Appendix A for a predicted cavity radius of 24.7 meters. The swell factor, n, used in the computation, was based on the observed chimney volume for Hardhat in relation to the in situ volume of rock which filled the available space following cavity collapse. This factor was 1.35, as computed from the equations given in Appendix A.

2.2.5 Depth of Spalling. Predictions of the lowest limit of spalling for the Shoal event were obtained by analog computation. The spall depths and thickness of the relatively undisturbed section predicted therefore differed slightly from that previously quoted (Reference 13) but the conclusions as to containment remained valid.

Since the number and depth of any spalls calculated are extremely dependent on the tensile strength that is

assumed for the medium, various cases were analyzed by analog computations for the Shoal event. A peak pressure pulse reflected at the surface equal to 210 bars (resulting from a yield of 14.26 kt) was assumed, and the tensile strength was varied from 6.9 to 82.7 bars in 6.9 bar steps to determine its effect on spalling depth. The peak pressure due to a 12.5 kt yield varies only slightly from the above, so the calculations remained valid.

The graphical plot of the data (Figure 2.3) shows the variation in depth and number of spalls as a function of tensile strength. It may be seen that no spalls occur when the tensile strength exceeds approximately 75.9 bars, and the deepest spalling occurs when the assumed strength is around 13.8 bars. The analog computations were checked and found to agree with those obtained graphically for 27.6 bars. One could then have said that, regardless of the tensile strength, the worst depth of spalling should be about 122 meters below the surface. This lower limit would leave a relatively undisturbed section of 134 meters between it and the top of the predicted chimney.

2.2.6 Radius of Spalling. To determine the distance out to which surface damage would occur, the lateral extent of spalling from surface zero was investigated. The exact determination of this radius was not obtainable by analytic methods, but estimates were obtained by comparing

the predicted surface displacements with those for an event where the spalling radius was known. For Hardhat the observed surface zero displacement due to spalling was 69.9 cm and spalling extended laterally between 457 and 914 meters (Reference 14). Displacements dropped off rapidly as the horizontal distance from surface zero increased. At 457 meters only 2.5 cm was observed. For Shoal the surface zero displacement was predicted to be 47.7 cm, which was less than that for Hardhat. Since the decrease in surface displacement with distance was assumed to be similar to that for Hardhat, the lateral extent of spalling was predicted to be of about the same magnitude, or less than 914 meters.

2.2.7 Elastic Radius. The elastic radius was predicted to occur between a radius of 253 to 286 meters. Prediction of the elastic radius becomes important in the determination of the attenuation rates for the propagated seismic signal. From an examination of empirical data, a distinct decrease in the attenuation is noticed on acceleration and particle velocity records at a particular distance from ground zero. This point may be accepted as the elastic limit and may be determined by considering the predicted pressures or particle velocities in relation to the properties of the medium.

Hydrodynamic calculations indicated that by a process

of convergence of the propagation velocity upon a final value (i.e., the limit of hydrodynamic action), an elastic radius would be determined to be about 253 meters. A similar computation for Hardhat yielded a radius of 230 meters, which was in general agreement with that observed. From an examination of the regression lines for particle velocity at Hardhat by the Sandia Corporation (Reference 15), a break point was indicated at a particle velocity of about 2.13 m/sec and a range of 222 meters. A possible additional check was made by scaling up this distance to the Shoal yield giving a prediction of 286 meters as the elastic limit.

Some doubt may be entertained as to whether the elastic limit is a distinct point or rather a range of pressures or particle velocities over which a change in attenuation occurs. The assignment of a discrete radius was therefore extremely tenuous and the elastic limit was considered as occurring approximately within a zone given by the radii shown above (253 to 286 meters).

2.2.8 Tunnel Closure Radius. Tunnel closure for the Hardhat event was continuous from the end of the drift out to station 3 + 90 (Reference 8), a radial distance of 128 meters from the W.P. Using this value as the parameter for cube-root scaling, a prediction of 164 meters was obtained as the outer limit of complete tunnel

closure for Shoal. As in the case of continuous tunnel damage, closure is dependent upon the pre-shot local geology to a large extent. Since the ground out to station 3 + 85 was highly fractured, the possibility of closure to 187 meters was not considered unlikely. With this in mind, and the fact that some closure at Hardhat occurred at 137 meters in a fault zone (Reference 8), closure for Shoal was anticipated to a radial distance of 187 meters.

2.2.9 Tunnel Damage Radius. The extent of damage to tunnels and shafts arising from a subsurface detonation is a function of the pre-shot geologic condition, physical properties of the medium, the angle of incidence and any support features employed. Radii quoted in Section 2.2.8 for this terminal effect considered these factors and indicated a range over which this damage would occur. However, since it is more useful to indicate a specific distance and the factors affecting possible variations, a more comprehensive procedure was employed. The availability of empirical data from Hardhat, an event in granite with an essentially similar configuration, provided the basis for prediction of effects by cube-root scaling without the omission of extenuating fact

Continuous damage in the Hardhat access tunnel

extended to station 2 + 47, a radial distance of about 172 meters from the shot point (Reference 8). The heavy damage between stations 2 + 90 and 3 + 40 was attributed to incompetent pre-shot conditions produced by a fault zone in this region. The radius of continuous tunnel damage for Hardhat was 172 meters. Using this value, by cube-root scaling, a damage distance of 221 meters was predicted for Shoal. It was considered possible that the presence of a highly fractured and faulted zone at a range of 232 to 258 meters might increase this predicted distance but the amount was not subject to accurate computation.

2.2.10 Predictions on Stemming. The evaluation of the stemming plan for Shoal contained in this report was based on the information contained in Reference 16. Consideration was also given to further details contained in other construction and support criteria. The yield used was the measured value of 12.5 kt as stated in Reference 17. The depth of W.P. was 366 meters, and the location was 6.1 meters south of core hole ECH-D. At the NVOO meeting on acceptability September 7, 1962, the criterion established by NVOO was that venting should not exceed that of the Gnome and Hardhat events.

Since the Hardhat event was the only U.S. nuclear explosion in granite, a comparison was made of the

effects of that event and those which were anticipated for the Shoal event. In both cases the chamber sizes were very small. Accordingly, the effect of chamber volume was not an important factor in comparing the two events.

The design for emplacement of the device vertically over the access drift instead of to one side was new. Also, there were a number of features of particular interest. The device was placed in a 38.1 cm diameter horizontal hole 6.1 meters from the W.P. and stemmed with sand. This arrangement was considered comparable to the explosion of a device in a drilled hole. The stemmed hole and sand near the W.P. was considered to provide effective initial stemming.

The back or top of the access tunnel directly below the proposed device emplacement locations, Station 10 + 00, was at a distance of 9.15 meters from the center of the explosion. Calculations indicated that the tunnel would be closed before any blast effects could reach this location by the longer path through Plug #1, down the raise and back to Station 10 + 00. The fact that sand stemming originally proposed in the raise was omitted was not expected to adversely affect the performance of the self-sealing arrangement.

The minimum yield that would produce closure was

computed on the basis of equal impulse to be 0.02 kt. The methods of computations for such small yields were open to question. However, even if the yield were very small, it was considered that the series of plugs would be adequate to contain the explosion.

2.2.11 Effectiveness of Plugs in Access Drift. The effectiveness of plugs is related to the damage radii anticipated. The four sand-fill plugs were at distances along the drift of approximately 6.1, 27.4, 45.7 and 76.2 meters from the point opposite the W.P. The latter two were much closer scaled radial distances than the sand plugs at Hardhat. These were located at approximate distances of 84 and 110 meters. Experience at Hardhat relative to the latter plug indicated that inward movement of rock compressed the plug thereby increasing its effectiveness. However, following cavity collapse predicted for Shoal), radioactive gases permeated the broken granite and entered the access tunnel beyond the last plug. These gases were largely contained by the gas seal door which was located approximately 234 meters from the W.P. At Shoal similar effects were considered probable but Plug #7 in the shaft was felt to be sufficient to filter out any radioactive particulate matter that might reach this area and thus minimize escape of radioactive gases to the surface.

2.2.12 Conclusions. As a result of evaluation of Reference 16 and subsequent data, conclusions were as follows:

1. There would be damage to the access drift beyond the last plug in the access drift with a high probability of contamination of that portion of the drift.
2. The 30.5 meter sand plug at the bottom of the shaft would prevent radioactive particulate matter from reaching that portion of the shaft above the plug and reduce the venting of radioactive gases to an acceptable level.
3. Damage to the shaft would necessitate remedial measures comparable to those for Hardhat if re-entry were made.
4. Geologic conditions were less favorable for containment than at Hardhat in that faulting and fracturing were extensive. This would be a factor in damage -- generally increasing damage where faults exist.
5. The stemming plan was generally adequate to reduce venting to a level less than observed at the Gnome and Hardhat events.

2.2.13 Evaluation of Possibility of Steam-Generated Secondary Explosion. Since hydrologic conditions at Shoal

were not accurately known (see page 14), the presence of water-bearing zones in the vicinity of the W.P. was assumed and possible effects were investigated. A review of the probable temperature-pressure history of the cavity was first made. This showed that initially the cavity would be filled with vaporized granite and water in the form of steam, the water being obtained from fixed water in the granite, all at extremely high temperature and pressure. Almost immediately the temperature would drop to a level where vaporized granite would condense. At the end of this phase the cavity would be filled with steam and there would be molten granite on the side walls and probably collected in a pool at the bottom. The temperature would then continue to be reduced by heat transfer to surrounding rock until a plateau was reached, when the granite started to solidify. The reason for the plateau is that as the granite solidifies, it gives up its heat of fusion, slowing down the general cooling. This temperature would be about 704 degrees C, the approximate melting point of granite (Reference 18).

Consideration was then given to the situation existing when the temperature remains at 704 degrees C during the period in which solidification of molten granite was proceeding at a relatively slow rate. As pointed out above, all the vaporized rock (and metal

from the device) would have been condensed. The device was placed in a 38.1 cm hole which was tamped; therefore, there should be very little air in the cavity. Only steam produced from water contained in vaporized or molten rock would remain. It was believed that the fixed water in the rock which was displaced radially would not be released.

Assuming that cavity collapse had not occurred, a computation was made as shown in Appendix B. This was for a 25.9 meter radius cavity but was also valid for a 24.7 meter radius predicted for a yield of 12.5 kt. Of particular interest was the conclusion that after vaporized rock has condensed, the cavity is filled with steam at 704 degrees C and the pressure would only be .345 bar absolute. In Reference 19, a post-shot evaluation of Rainier, it is hypothesized that a pressure drop occurred because steam escaped from the cavity through fissures. (Since there was no report of venting, this assumption of escape of steam may not be justified.) The occurrence of the pressure drop is based on examination of vesiculated material. It is stated on page 4, Reference 19, that, "Thus, the evidence strongly points to the fact that the vapor pressure was 40 atmospheres inside the chamber immediately after the shot while glass droplets were still falling from the roof of the chamber; a minute or two later the pressure had dropped to a few atmospheres."

The drop of pressure to a low value immediately after the explosion was considered to be a factor in cavity collapse.

The spalling of pieces of rock from the surface of the cavity by steam forming behind the face would be accelerated by the low pressure. However, the analysis indicated that an influx of a large volume of water within a particular length of time would be required to cause the pressure to rise to 6.9 bars. At the assumed rate of flow of 265.0 liter/min, 7 hours would be required. If a larger flow was assumed the time would be reduced proportionately. Although precise procedures for analysis of the rates of heat transfer were not developed, an approximate analysis indicated that the inflow of water would have a net cooling effect on the heated rock in and surrounding the cavity.

The above discussion assumed that the cavity would not collapse before the pressure was reduced to the point where water might enter. Since at Hardhat, cavity collapse did not occur until 11 hours after the event (Reference 7), this was a reasonable assumption. It was assumed that cavity collapse was unlikely until the pressure in the cavity was reduced to a value less than the lithostatic pressure, 82.7 bars. If collapse occurred when the cavity pressure was somewhat greater than 6.9 bars, cooling should have proceeded at a rapid rate from

the effect of the relatively cool rock masses falling into the cavity.

The only other concern was that water entering tunnels in the vicinity of the shot point may have been heated by the effect of the explosion. Consideration of the limited heat available in such a case indicated that relatively small quantities of steam would be generated. While such an explosion might have had a local effect, it was felt unlikely that it could affect containment. Passage of the steam through access tunnel plugs was considered improbable. If it did vent into the access tunnel, condensation would reduce the pressure materially before the steam reached the 30.5 meter plug in the shaft. This massive plug was felt sufficient to effectively prevent any steam escaping to the atmosphere.

On the basis of the above discussion, the following conclusions were reached:

1. Evidence suggested that ground water may have existed in the vicinity of the W.P.
2. Following the condensation of vaporized rock and metal from the device, the steam pressure in the cavity was expected to be very low, less than one bar. When the shell of melted rock was broken by implosion of portions of the shell by steam in pockets behind the face, an inflow

of water would occur slowly, raising the steam pressure and cooling the rock. The pressure was considered to be limited to 6.9 bars as any increase above that pressure would prevent further inflow of water.

3. Should the cavity collapse, temperatures and pressures would be lower than at the time rock is solidifying. Rapid cooling from introduction of broken rock would reduce temperatures and pressures rapidly.
4. Entry of water into heated tunnels or other openings near the W.P. might cause localized explosions. Condensation of steam in passageways and the 30.5 meter plug in the shaft would have prevented steam reaching the surface.
5. Finally, no significant hazard existed from secondary explosion by entry of ground water into the cavity.

2.2.14 Estimate of Prompt Venting of Gaseous Isotopes. It was estimated that prompt venting of radioactive isotopes to the surface through fissures was unlikely for reasons stated below. The possibility of venting through stemming is discussed in Section 2.2.12.

It was predicted that surface spalling would extend to a depth at Surface Zero not greater than 122 meters.

Prior to the collapse of the cavity (which, on the basis of experience in Hardhat, would be delayed) there would remain above the cavity a thickness of 366 - (25.9 + 122) = 218 meters of relatively undisturbed rock. All holes from the surface were reported to have been grouted to prevent escape of radioactive gases to the surface. Drilling in the vicinity of the W. P. established the fact there were no faults within a radial distance of 30.5 meters. Under these conditions the displacement of material radially from the W. P. would compress the gouge in the fault and inhibit the escape of radioactive gases through Fault Zone E at a radial distance of about 34 meters.

The possibility of immediate escape of radioactive gases through a thickness of 218 meters appeared to be extremely remote. In the first place the very small diameter of the chamber assured the maximum degree of melting of the granite. The molten layer at the periphery of the cavity was felt to be impervious to the escape of gases as the tendency would be to drive the molten material into any fissures which might exist and close them. Such action is indicated in tuff (Reference 19). However, as cooling occurs, post-shot observations of Rainier indicate that the wall material is imploded into the cavity (Reference 19). This is believed to be caused by steam pressure behind the surface. Since granite has a much smaller

quantity of moisture and greater competence, it was considered unlikely that such implosion would occur to the same extent or as rapidly. This is substantiated by the fact that no radiation was detected at Rainier's Surface Zero until H + 1 hour at which time it was only 10 mr/hr (Reference 19).

As a further consideration, estimates of the small amount of water available for generation of steam indicated that pressures ir the cavity should be very low following condensation of gaseous rock, which should occur rapidly. This was important as there would be insufficient pressure in the cavity to force radioactive gases up through the overlying rock (see Section 2.2.13).

2.2.15 Prediction of Containment. It was predicted that the Shoal event would be contained to the same degree as the Hardhat event for reasons discussed below.

Containment of the explosion at the time of the event depends upon adequacy of stemming, depth of burst, and absence of passages which could provide a path for radioactive venting. Following the explosion, some of the wall material was expected to implode, breaking the seal formed by the melting of a shell of rock at the periphery of the cavity. This would permit the escape of some radioactive gases into fissures in the rock.

After the cavity collapsed, a different situation

would exist. A chimney having a height of 110 meters measured from the elevation of the W.P. was predicted. A depth of spalling not to exceed 122 meters was predicted. Thus, there would remain a thickness of 366 - (110 + 122) = 134 meters of relatively undisturbed rock as a barrier against escape of radioactive gases to the surface. It was assumed that the temperatures and pressures would have been markedly reduced by the collapse of the cavity and the filling of the cavity with rubble at the ambient temperature of the rock (except for that portion adjacent to the cavity). Therefore, any possible escape of radioactive gases to the surface would be more in the nature of a low-pressure migration or diffusion. Radioactive isotopes that condense at ambient temperatures should not reach the surface. There remain xenon and krypton which might possibly escape to the surface at a slow rate.

Stemming, as discussed in Section 2.2.10, was predicted to be adequate for the immediate period of the explosion and that following cavity collapse.

2.3 SEISMIC EFFECTS

Predictions of particle motions, for the Shoal model described in Chapter 1, were made using the equations given below.

2.3.1 Acceleration. The particle acceleration equation was developed through use of a least-squares equation for three components of surface peak particle

acceleration for tuff which was adjusted to fit the value of acceleration observed at the Las Vegas Seismic Safety Net Station from the Clearwater event.

The least-squares equation was:

$$a - 3.2 \times 10^{6} W^{.7} R^{-2.0} \text{ (Reference 20)} \quad (2.3.1)$$

where

a is in units of gravity

W is in kilotons

R is in feet

or for R in meters,

$$a = 2.96 \times 10^{5} W^{.7} R^{-2.0} \quad (2.3.2)$$

Computation of peak surface particle acceleration using equation 2.3.2, the Clearwater-Las Vegas distance in meters and the reported yield for Clearwater yielded a value lower than the recorded 0.0005 g (Reference 21). To rectify the discrepancy, the coefficient of equation 2.3.2 was adjusted to fit the observed value by substituting the observed Clearwater-Las Vegas results in the equation:

$$a = K W^{.7} R^{-2.0} \quad (2.3.3)$$

The value of the coefficient, K, obtained from equation 2.3.3 is 5.03×10^{5} which, when substituted above, yields the equation:

$$a = 5.03 \times 10^{5} W^{.7} R^{-2.0} \quad (2.3.4)$$

This was used to predict surface particle acceleration for the Shoal event (see Figure 2.4 and Table 2.2).

2.3.2 Displacement. The displacement equation is that reported in Reference 22 as:

$$\text{Log } A = 0.75 \text{ Log } Y - 1.73 \text{ Log } R \qquad (2.3.5)$$

which, rewritten in exponential form, is:

$$d = W^{.75} R^{-1.73} \qquad (2.3.6)$$

where

d = surface displacement in centimeters

W = yield in kilotons

R = distance in kilometers

or for R in meters,

$$d = 1.51 \times 10^{5} W^{.75} R^{-1.73} \qquad (2.3.7)$$

The peak surface particle displacement predicted at Las Vegas for the Clearwater event was 0.004 cm. Since a value of 0.003 cm (Reference 21) was observed for a lower yield, equation 2.3.7 was used to predict the displacements expected from the Shoal event (see Figure 2.5 and Table 2.2).

2.3.3 Velocity. Data for peak surface particle velocity, of a reliability equal to that of acceleration and displacement data in the range of interest, were not available. Accordingly, simple harmonic motion was assumed and an equation for particle velocity was obtained through use of the relationship:

$$u = \left[K(ad)\right]^{.5} \qquad (2.3.8)$$

where

K = gravitational constant - 980 centimeters/second/second

u = peak surface particle velocity in centimeters/second

a = peak surface particle acceleration in g's

d = peak surface particle displacement in centimeters.

The values of acceleration and displacement substituted in equation 2.3.8 are obtained from prediction equations 2.3.4 and 2.3.7 given above. The resulting peak surface particle velocity equation is:

$$u = 8.64 \times 10^{6} \, W^{.73} \, R^{-1.87} \qquad (2.3.9)$$

This equation was used to predict particle velocity for Shoal (see Figure 2.6 and Table 2.2).

2.3.4 Equations in Terms of Particle Motion. Equations 2.3.4, 2.3.7 and 2.3.9 may be rewritten in order to obtain distance to any particular motion of interest. These are:

$$R = \left[\frac{5.03 \times 10^{5} \, W^{.7}}{a}\right]^{.50} \qquad (2.3.10)$$

$$R = \left[\frac{1.51 \times 10^{5} \, W^{.75}}{d}\right]^{.58} \qquad (2.3.11)$$

$$R = \left[\frac{8.64 \times 10^{6} \, W^{.73}}{u}\right]^{.54} \qquad (2.3.12)$$

where

R = distance in meters

W = yield in kilotons

a = peak surface particle acceleration in units of gravity (g)

d = peak surface particle displacement in centimeters

u = peak surface particle velocity in centimeters/second

Equations 2.3.10 and 2.3.12 have been used in computing distance to 0.1 g and 11 cm/sec for radius of damage as shown in Figure 2.7 and distance to 0.001 g for limit of perceptibility in the same figure.

CHAPTER III

ANALYSIS AND INTERPRETATION

3.1 PHENOMENOLOGY AND CONTAINMENT

As stated in Chapter 2, prediction of effects and an evaluation of containment were made for the purposes of operational safety. Limited post-shot exploration permits a comparison of only some of the predicted quantities with observed values. The primary result of the Shoal event was that it was satisfactorily contained as predicted. The prediction of containment was based on an estimation and analysis of the individual effects anticipated and the interrelation of one to another with respect to containment.

3.1.1 Cavity Radius. The post-shot cavity radius as determined by drilling was 25.6 $\pm$ .6 meters (Reference 17). This compares very well with the predicted radius of 24.7 meters, confirming the procedure of scaling Hardhat results to the Shoal yield.

3.1.2 Chimney Height. The post-shot chimney height was found to be 108 meters (Reference 17). The predicted value was 110 meters. This close agreement substantiates the granite swell factor and other assumptions used to determine the extent of chimney formation.

3.1.3 Depth of Spalling. The lowest limit of spalling was predicted to be 122 meters below the surface. Exact post-shot data are not available but indications are that spalling extended below 120 meters. It has been stated (Reference 23) that an examination of records from gages vertically over the shot point indicated that free fall occured at a depth of 85.5 meters. It was also believed that free fall occurred at a depth of 120 meters but owing to gage difficulties this is not positive. The cable leading to the accelerometer broke at 0.3 seconds providing only a partial record. The velocity gage gave a continuous record and the slope indicated free fall but the period was so short that a positive interpretation cannot be made.

3.1.4 Radius of Spalling. The lateral extent of spalling from surface zero was predicted to be less than 914 meters. This has been shown to be close to the observed radius by the results given in Reference 24. From aerial examination it was found that intense fracturing was confined to within 107 meters of surface zero. Fractures up to 1.3 cm wide occurred out to 458 meters south, 794 meters north, 366 meters east and 610 meters west;

some fractures in this zone were as wide as 15 cm. It is felt that these fractures are indicative of the radii to which spalling occurred and are in agreement with the prediction thus providing substantiation for the procedures used.

The above-mentioned effects were all used to arrive at the conclusion that the Shoal event would be contained. Additionally, an evaluation of the stemming plan showed it to be adequate. Both of these conclusions were completely substantiated by the results of the test.

Several predicted effects such as cracking radius, radius of radioactive injection into cracks and tunnel damage predictions can not be substantiated accurately due to the lack of post-shot data at this time.

3.2 SEISMIC EFFECTS

As detailed in Chapter 1, surface motions resulting from the Shoal event were recorded at various locations with acceleration, displacement, and/or velocity-sensitive instruments. The resulting records have been corrected for the particular instrument transfer function to obtain true ground motion neglecting instrument to ground coupling. Additionally, the corrected acceleration and

displacement records have been integrated and differentiated respectively to obtain surface particle velocity where direct measurements of this parameter were not made. Peak values of surface particle motion have been determined from the corrected records. In addition, the available components at each station have been analyzed simultaneously in order to determine the absolute values of peak motion received at the station. These values are denoted as peak resultant vectors.

In order to evaluate the specific objectives stated in Chapter I, the peak motions have been segregated into classifications on the basis of parameter of motion measured, component measured, station lithology and relation of station location to areal geology. All peak motions, both directly measured and derived, are given in Tables 3.1 through 3.3. In view of the fact that funds for accomplishment of detailed analyses of data were delayed, it is not practicable to include such results in this report. A research report covering the analyses of Shoal data and that from other events will be submitted when detailed analyses have been completed. The preliminary analysis and interpretation of results presented here are given on an objective-by-objective basis.

3.2.1 The Variation in Amplitude of Ground Motions on Granite and Alluvium with Distance. Figures 3.1 through 3.12 show peak surface resultant vectors and individual components of ground motion recorded on granite and alluvium from the Shoal event by the USC&GS. Besides the recorded values, the graphs show the least-square regression equation derived from the data and the standard error of estimate (which will be discussed in detail in Section 3.2.6, below).

The data recorded on alluvium show consistently larger particle motions than that recorded on granite. The rates of attenuation for the two media are nearly the same. Sufficient measurements were made to allow an approximation of the magnitude of amplification caused by the presence of alluvium. Although some differences in rates of attenuation between granite and alluvium measurements are evident (see Figures 3.1 through 3.4) and the overlap of data with distance is small, it can be seen that peak accelerations on alluvium are larger than peak accelerations on granite by an average factor of 2.1. Similarly, for displacement (Figures 3.5 through 3.8) the factor averaged 3.7 and for velocity (Figures 3.9-3.12) 3.4.

3.2.2 The Effect of Faulting on Ground Motion. Peak resultant vectors of particle motion measured on instrument lines parallel to the major northeast-southwest fault trend have been compared with those measured on lines perpendicular to the faulting. The orientation of applicable stations with respect to the fault trend are listed in Table 3.4. Figures 3.13 through 3.15 show data points and the associated least-squares regression lines for lines parallel and perpendicular to the fault trend. These figures show a trend to higher rates of attenuation perpendicular to the faulting than are seen parallel to the faulting. However, the evidence is not sufficiently strong to state that there is a definite difference in attenuation due to energy transmission across fault systems.

3.2.3 The Effect of Thickness of Alluvium on the Amplitude and Attenuation of Amplitude with Distance. This effect may be best examined for Shoal by comparing data recorded on the thick alluvium of Fairview Valley to the east of the Sand Springs Range with that recorded on Fourmile and Eightmile Flats to the west of the Sand Springs Range where the alluvium wedges out against the

underlying granite. However, insufficient data were obtained to make a meaningful statistical evaluation of this effect.

3.2.4 The Partition of Compressional Wave Energy into Surface Waves at a Lithologic Discontinuity. As seen in Figures 3.1 through 3.12, the rates of attenuation for stations on alluvium are nearly the same as those for stations on granite. This seems to indicate that even though thick alluvium is present, the peak motions measured on alluvium were the result of the same type of wave that produced peak motions at the granite stations. The rates of attenuation observed on alluvium from the Shoal event are considerably higher (with the exception of the transverse component) than the attenuation rate observed for surface-type waves generated by twenty-eight events at Yucca Flat (Reference 25). Therefore, it is probable that all peak motions recorded at Shoal were the result of body waves which in the presence of thick alluvium have been amplified by the factors discussed in Section 3.2.1, above. Because of this, no determination of energy partition between body and surface waves at a lithologic discontinuity can be made. It is important

to note that the above discussion is based on peak amplitudes measured by instruments which respond best to periods of four seconds or less. The intent is not to say that long period surface waves, possibly of large amplitude, did not occur; but rather that there was no evidence from these particular instruments that this type wave produced any peak motions.

3.2.5 The Directional Response Characteristics of the Shot Medium. The azimuthal variations of amplitude in the Sand Springs Range appear to be controlled to a certain extent by the major fault trend in the range (see Section 3.2.2, above). Analysis has not indicated any azimuthal variations due to inherent properties of the shot media, i.e., granite, separately from the effects attributed to faulting.

3.2.6 The Degree of Scatter in Recorded Ground Motions. The degree of scatter is difficult to judge without the use of statistical analysis. A convenient numerical quantity is the standard error of estimate (σ_y) which can be determined during the regression analysis. This is a multiplicative factor -- additive in logarithmic form -- and has the following significance.

Assuming normal distribution of data points used in the regression analysis, a band width of 1 σ_y on either side of the regression line will include about 68 percent of the data points. A band of $\pm$ 2 σ_y or 3 σ_y will include about 95 percent or 99 percent, respectively, of the data points. Standard errors are multiplicative because of the form of the equation which has been used:

$$PM = KR^{-n}$$

where

PM = peak particle motion in g, cm, or cm/sec depending on type of motion

R = distance in meters

K, n = constants determined by regression analysis

This equation is linear in logarithmic form

$$\log PM = \log K - n \log R.$$

The standard error of estimate is derived from this linear equation and is itself a logarithm. Therefore, $\log PM \pm \log \sigma_y$ means $(PM)(\sigma_y)$ or PM/σ_y.

The 1 σ_y band width is shown on the graphs and the value of σ_y is presented with the equations. In all cases where the regression equation is statistically significant, the value of σ_y is less than two. Thus,

the equations represent, within a factor of less than two, some 68 percent of the data values recorded if normal distribution is assumed.

3.2.7 The Ratio of (u^2/ad) Where u is Particle Velocity, a is Particle Acceleration, and d is Particle Displacement. This ratio was examined for the three stations at which independent measurements of the three ground motion parameters were made. These data are listed in Table 3.5. The computed ratios vary from .076 to .68. However, insufficient data were available to make meaningful statements about ratios associated with specific components.

3.2.8 Comparison of Observed Data with Predictions. Figures 3.16 through 3.18 show the comparison between equations used for predicting Shoal surface motions and the least-square regression lines for observed peak resultant vectors. All prediction equations are higher than the least-square fits for hardrock. The acceleration and displacement predictions are no higher than the $+1\ \sigma_y$ level and have slopes slightly in excess of those observed. The velocity prediction is higher than the hardrock-observed peak resultant vectors by a factor of

about two with nearly equivalent slopes. In all three comparisons the equations for data observed on alluvium are higher than the prediction equations by factors in the range of 1.5 to 4.0.

On the basis of this comparison, it is believed that the prediction equations for acceleration and displacement adequately represent a reasonable upper limit of motion measured on hardrock. The prediction equation for velocity is felt to be too high. If the +1 σ_y level is assumed to be a reasonable upper limit, then the coefficient of the velocity prediction equation is too high by an average factor of 1.6.

Based on this data, the prediction equations which will be used for future events in granite will be as follows:

for points of interest on hardrock

$$a = 5.03 \times 10^5 \, W^{.7} \, R^{-2.0}$$

$$d = 1.51 \times 10^5 \, W^{.75} \, R^{-1.73}$$

$$u = 5.40 \times 10^6 \, W^{.73} \, R^{-1.87}$$

for points of interest on alluvium

$$a = 1.06 \times 10^6 \, W^{.7} \, R^{-2.0}$$

$$d = 5.59 \times 10^5 \, W^{.75} \, R^{-1.73}$$

$$u = 1.84 \times 10^7 \, W^{.73} \, R^{-1.87}$$

where units are:

a = acceleration in g

d = displacement in cm

u = particle velocity in cm/sec

W = yield in kt

R = distance in meters

Future research and analysis may allow revision of the above equations so as to include variables (e.g., frequency) whose effect is not reflected in current prediction equations.

CHAPTER IV

CONCLUSIONS AND RECOMMENDATIONS

Detonation of the 12.5 kt Shoal event in granite has provided much needed information on seismic effects relating to public safety. In addition to being the best-instrumented shot to date in granite, Shoal also provided the first sufficient amount of data for comparing the amplitudes of ground motions measured on hardrock with those measured on alluvium.

The regression data are considered to be reasonably reliable as evidenced by the values obtained for the standard error of estimates.

It appears that peak motions on the alluvium are due to the same type of wave as peak motions on hardrock.

The equations used by Roland F. Beers, Inc. to make predictions agree well with observations.

The evaluation of containment for the Shoal event and the adequacy of the stemming plan were substantiated by the results of the test. Limited post-shot exploration indicated that predictions of cavity radius, chimney height, depth of spalling, and radius of spalling were accurate. More extensive post-shot exploration would permit

comparisons of other predicted effects which could not be evaluated presently.

Details of data processing methods and studies of a long-range research nature will be published in a separate report.

APPENDIX A

ANALYSIS OF SPALLING MECHANISM

Spalling is herein defined as the fracturing of a solid by tensional stresses produced when a seismic pulse is reflected from a free face. The conversion of a compressional pulse to a tensional one is considered to be perfectly elastic with no loss of energy into the atmosphere at the solid-air interface.

The problem is to analyze the stress situation at continuous distances back from the free face to determine if sufficient tension exists to fracture the solid. The tensional stress arises only from the reflected pulse, whereas those forces resisting fracturing are that portion of the compressional pulse waveform which has not yet arrived at the interface, the tensile strength of the medium, and any overburden pressure which becomes significant when horizontal surfaces and long wave lengths are considered.

If the problem is restricted to one involving compressional pulses arising from subsurface nuclear detonations and a rock medium, generalized equations may be used to determine the stress condition at continuous depths

below the surface. The equations are based on hydrodynamic considerations and machine computations; in the form shown they are applicable at ranges of a few hundred meters. The pulse shape assumed is one with an exponential decay thus producing a maximum pressure the instant the peak reaches a point of interest. The stress condition at any point below the surface may then be given by:

$$P_{net} = P_{ovb} + P_{ts} + P_{pwf} - P_{ref}$$

where

P_{net} - net stress at the section of interest

P_{ts} = constant - tensile strength of the medium

P_{ovb} = K (depth) - overburden stress

$P_{pwf} = P_p \left(\frac{r}{R}\right)^2$ - pressure wave form, or that portion of the pulse which has not arrived at the free surface

$P_{ref} = CR^{-1.5}$ - reflected peak pressure

where

R = depth of burial + the depth of interest

r = depth of burial - the depth of interest

The value of each of these quantities may then be computed as functions of depth to determine if P_{net} becomes $\geq$ zero, in which case a spall is predicted to occur. When

a spall occurs, the overburden pressure must be reduced to zero since the overlying strata are detached, and recomputed for further depths of interest on the basis of the newly created free surface. Additionally, the peak reflected pressure P_{ref} must be reduced to the value of the pressure wave form P_{pwf} at the new free face since the energy in the descending pulse is trapped in the spalled section. On the basis of these new values further depths of interest may be investigated to determine if additional spalls will occur.

Since actual test conditions are not similar to free-field predictions for a homogeneous medium, corrections for the variation in the stratigraphic section are introduced. The transmission coefficient, or change of pressure across an interface, is given by:

$$\frac{P_2}{P_1} = \frac{2\rho_1 C_1}{\rho_1 C_1 + \rho_2 C_2}$$

where ρ_1 is the density and C_1 is the compressional wave propagation velocity of the original medium and ρ_2, C_2 are those of the medium across the interface. Corrections for transmission coefficients must be introduced at all depths where they are applicable, to both the ascending

and descending pulses.

The analysis as outlined above is confined to the case of normal incidence only and three methods are presently available for the solution of the calculations; these are by graphical procedures, analog computer and digital computer.

POST-SHOT CHIMNEY CALCULATIONS

Calculations to determine the height to which post-shot chimney formation will occur are based on the assumption that:

1) The post-shot cavity is spherically symmetrical,
2) The chimney is cylindrical with a radius equal to that of the cavity, and
3) An increase in volume will occur upon breaking of solid material.

The volume of the cavity, or void, is

$$V_{cav} = 4/3\ \pi\ R^3$$

The volume of the chimney (V_{ch}) is then given by

$$V_{ch} = \pi\ R^2 h$$

where

h = the height above the working point

Since the chimney volume includes one half of the cavity void, the volume of solids is seen to be:

$$V_{sol} = V_{ch} - \tfrac{1}{2} V_{cav}$$

The original volume of solid material must then swell upon breaking to include both its original volume and the volume of the existing void

$$(n)\ V_{sol} = V_{cav} + V_{sol}$$

where

(n) = the swell factor for the medium being considered.

Then $n \left[\pi R^2 h - 2/3\ \pi R^3\right] = 4/3\ \pi R^3 + \pi R^2 h - 2/3\ \pi R^3$

and $n\ (h - 2/3\ R) = 2/3\ R + h$

yielding $n = \frac{h + 2/3\ R}{h - 2/3\ R}$ and $h = \frac{2/3\ R\ (1+n)}{n-1}$.

The value of (n) may then be determined for mediums in which experience is available and subsequently be used to determine the chimney height for future events, in the same medium, based on the predicted cavity radius.

PERMANENT DISPLACEMENT AND STRAIN CALCULATIONS

With the detonation of an underground nuclear explosion a post-shot cavity results which is larger than the original shot chamber. The expansion of this cavity to

its final size entails the vaporization, melting and deformation of the material surrounding the original chamber. The major portion of the material is displaced radially from the source. The difference in position between an original point in the medium and its final location, as measured upon re-entry, is termed the permanent radial displacement of the point.

EQUATION DERIVATION

Given the initial chamber radius and final cavity size, the assumption can be made that the medium has behaved as an incompressible material and no loss of volume of material has occurred through vaporization or melting. The volume of material which originally occupied the post-shot cavity must, therefore, be distributed throughout the medium. Assuming spherical symmetry the following equation may be derived:

Given: R_1 = radius of original shot chamber

R_1' = radius of post-shot cavity

R_2 = original radius to point of interest

R_2' = final radius to point of interest

If the original and final volumes are equal, then

$$4/3\ \pi\ \left[(R_2)^3 - (R_1)^3\right] = 4/3\ \pi\ \left[(R_2')^3 - (R_1')^3\right]$$

and $(R_2')^3 = (R_2)^3 - (R_1)^3 + (R_1')^3$ yielding $\Delta R_2 = R_2' - R_2$ which is the permanent radial displacement of a point whose initial position was R_2.

Given the predicted radial permanent displacements, the tangential strains may be computed by considering the change in circumference at any radius of interest.

The compressive strain due to a radial displacement is obtained by plotting the displacement versus distance, and fitting an equation to that segment of interest. At distances relevant to radial fracturing, this portion of the curve may be approximated by the equation $D = CR^{-1.9}$ meters. The radial strain is then $\frac{dD}{dR} = -1.9\ CR^{-2.9}$ meters/meters.

APPENDIX B

These data were computed for an anticipated maximum yield of 14.26 kt but are equally valid for 12.5 kt.

Basic data:

Depth of burial - 366 meters

Cavity radius - 2.59×10^{1} meters

Cavity volume - 7.3×10^{4} M^3

Fixed water content of Shoal granite - 3% by volume

Melting point of Shoal granite - 704° (Reference 18)

Grams of water per cubic meter of rock - 3.0×10^{5}

Depth to top of water table - 297 meters

Hydrostatic pressure at W.P. (366-297) (.1) = 6.9 bars

Density of granite - $\rho o = 2.67$ gm/cm^3

The following computation is made with the assumption that only the rock which was melted would release its fixed water.

Heat of fusion for granite - 100 cal/gm

Specific heat - 0.2

Ambient rock temperature assumed - 20°C

Sensible heat - 136 cal/gm

Enthalpy - 9.88×10^{9} ergs/gm @ 700°C

Waste heat density - 987.9×10^7 ergs/gm (2.67 gm/cm^3) = 2.64×10^{10} ergs/cm^3

From Hugoniot data for granite, this waste heat density occurs at a pressure of about 340 kilobars. This pressure has been determined from Beers, Inc. hydrodynamic computations to occur at a radius of 3.42×10^2 cm.

Volume of rock melted = $\frac{4 \pi (3.42^3)}{3}$ = 167 m^3

Volume of fixed water vaporized = 0.03 (167) = 5 m^3

Weight of water vaporized = $5 \times 1.0 \times 10^3 = 5.0 \times 10^3$ kg

Specific volume of water @ 704°C = $\frac{7.3 \times 10^4}{5.0 \times 10^3}$ = 14.6 m^3/kg

From steam tables for these conditions P = 0.35 bars

The above pressure of 0.35 bars is less than the hydrostatic pressure of 6.9 bars and would, therefore, be insufficient to keep out water.

At some point, steam pressure behind the impervious layer formed by the melted rock may be sufficient to cause pieces of this layer to break out into the cavity and water might enter. Assuming that water flows in at a rate comparable to that in the E-1 hole, the pressure would increase until it reaches 6.9 bars at which time inflow would be stopped by equalization of pressure. The time to reach this pressure may be computed as follows:

At 704°C, the specific volume at 6.9 bars absolute = 0.652 m^3/kg.

Weight of water = $\frac{7.3 \times 10^4}{6.52 \times 10^{-1}} = 1.12 \times 10^5$ kg

Additional water required $1.12 \times 10^5 - 5.0 \times 10^3 =$

1.07×10^5 kg

The October 4, 1963 NVOO Construction Progress Report shows Hole E-1 making 265 liter/min = 265 kg/min.

Time to reach 6.9 bars = $\frac{1.07 \times 10^5}{2.65 \times 10^2} = 404$ minutes $\approx$ 7 hours.

TABLE 2.1 COMPARISON OF PHYSICAL PROPERTIES OF SHOAL AND CLIMAX STOCK GRANITES

Physical Property	Shoal Granite				Climax Stock Granite			
	Average	Maximum	Minimum	References	Average	Maximum	Minimum	References
Bulk Density, gm/cm^3	2.52 2.64	2.54 2.645	2.40 2.626	(26) (9)	2.67	2.69	2.56	(29)
Compressional Velocity, 10^3 m/sec	5.40 5.16	5.52 5.20	5.27 5.12	(26) (9)	6.25	6.45	6.175	(30)
Shear Velocity, 10^3 m/sec	3.03	3.11	2.89	(26)	3.42	3.49	3.28	(30)
Poisson's Ratio	0.268	0.288	0.257	(26)	0.30	0.33	0.27	(30)
Shear Modulus, 10^5 bars	2.31	2.44	2.12	(26)	3.04	3.24	2.62	(30)
Bulk Modulus, 10^5 bars	4.28	4.64	4.08	(26)	--	--	--	
Young's Modulus, 10^5 bars	5.88 4.97 --	6.17 5.06 4.64	5.42 4.92 3.47	(26) (9) (1)	7.93	8.20	7.45	(30)
Thermal Conductivity 10^3 gm cal/sec/cm	3.8	4.5	3.1	(1)	--	--	--	
Heat of Fusion cal/gm	100[a]	--	--	(27)	100[a]	--	--	(28)
Compressive Strength 10^3 bars	1.10	1.18	1.05	(9)	1.27	2.02	0.849	(31)
Tensile Strength 10^1 bars	6.55	6.66	6.48	(9)	13.2	--	--	(32)
Fracture Strain, Percent	0.33[a]	0.45[a]	0.2[a]	(28)	0.33[a]	0.45[a]	0.2[a]	(28)

a An average figure for any typical granite

TABLE 2.2 PREDICTIONS OF AMPLITUDES OF GROUND MOTION

Peak Surface Particle Motions Expected at Locations of Interest - Shoal Event, 12.5 KT

Location	Distance (Meters)	Acceleration (g)	Displacement (cm)	Velocity (cm/sec)
Site Comm. Rep.	1,463	1.38	3.26	65.9
C.P.	2,240-2,360	.59-.53	1.61-1.47	29.7-26.9
Observation Post	2,440	.50	1.39	25.3
Onset Damage	3,900	--	--	11.0
Onset Damage	5,430	.10	--	--
Hwy 50	7,200-9,600	.057-.032	.21-.13	3.4-2.0
Frenchman's Sta.	12,900	.018	.078	1.1
Nev. Scheelite	20,900	.0068	.034	.46
Salt Wells	26,000	.0044	.023	.30
Fallon Tower	35,000	.0024	.014	.17
Limit Perceptibility	54,300	.0010	--	--

TABLE 3.1 PEAK SURFACE PARTICLE ACCELERATION IN g's

Station	Distance (meters)	Component			
		Vertical	Radial	Transverse	Resultant Vector
Hardrock					
1/2A	954	--	0.956	--	--
1A	1,500	0.639, 0.783	0.588, 0.650	0.253	0.650, 0.813
2A	3,125	0.176	0.139	0.0842	0.215
3A	4,920	0.0906	0.207	0.0913	0.219
1B	1,805	0.538	0.385	0.530,	0.589
2B	3,394	0.119	0.0716	0.0718	0.120
3B	4,887	0.0789	0.0461	0.0639	0.0850
4B	6,522	0.0315	0.0371	0.0313	0.0422
6B	9,668	0.0210	0.0120	0.00993	0.0226
1/2C	1,042	1.72	1.06	0.989	1.77
1C	1,794	0.817, 0.903	0.460, 0.516	0.381, 0.366	0.927, 0.914
2C	3,392	0.181	0.283	0.194	0.337
3 1/2C	5,706	--	0.0742	--	--
1D	1,493	0.703, 0.652	0.570, 0.527	0.266	0.735, 0.711
East 1	14,430	--	--	--	--
West 1	19,150	--	--	--	--
Mercury	27,650	--	--	--	--
North 2	29,000	--	--	--	--
East 2	39,900	--	--	--	--
Gabbs Mine	55,400	--	--	--	--
(Scheelite?)	20,400	--	--	--	--

TABLE 3.1 (cont.)

Station	Distance (meters)	Component			
		Vertical	Radial	Transverse	Resultant Vector
Alluvium					
4 1/2A	7,147	0.0753	0.0606	0.0454	0.0768
8A	12,820	--	0.0206	0.0223	--
12A	18,890	0.0171	0.00986	0.00850	0.0179
3D	4,720	0.344	0.114	0.109	0.346
4 1/2D	6,921	--	0.0509	0.0386	0.0562
9D	14,062	0.0303	0.0382	0.0293	0.0303
16D	25,431	--	0.0116	0.0116	0.0146
Naval Air Sta.	36,200	--	--	--	--
(Scheelite?)	20,400	--	--	--	--

TABLE 3.2 PEAK SURFACE PARTICLE DISPLACEMENT IN CENTIMETERS

Station	Distance (meters)	Component			
		Vertical	Radial	Transverse	Resultant Vector
Hardrock					
1 2A	954	--	--	--	--
1A	1,500	2.50, 3.46	1.93, 1.85	0.829, 0.719	2.56, 3.69
2A	3,125	1.08	0.634	--	1.16
3A	4,920	--	0.314	0.117	0.315
1B	1,805	--	2.09	2.66	3.28
2B	3,394	0.217	--	0.181	0.243
3B	4,887	--	--	--	--
4B	6,522	--	0.232	0.124	0.239
6B	9,668	--	0.127	0.0766	0.138
1/2C	1,042	2.73	2.50	--	2.74
1C	1,794	1.04, 1.26	0.830, 0.780	0.314, 0.324	1.24, 1.37
2C	3,392	0.572	0.554	--	--
3 1/2C	5,706	--	--	0.160	--
1D	1,493	--	1.92, 1.89	0.830, 0.742	1.92, 1.96
East 1	14,430	--	--	--	--
West 1	19,150	--	--	--	--
Mercury	27,650	--	--	--	--
North 2	29,000	--	--	--	--
East 2	39,900	--	--	--	--
Gabbs Mine	55,400	--	--	--	--
(Scheelite?)	20,400	--	--	--	--

TABLE 3.2 (cont.)

Station	Distance (meters)	Component			
		Vertical	Radial	Transverse	Resultant Vector
Alluvium					
4 1/2A	7,147	0.582	1.11	0.503	1.15
8A	12,820	--	0.353	--	--
12A	18,890	--	--	0.233	--
3D	4,720	0.544	0.936	0.411	0.988
4 1/2D	6,921	--	0.509	0.463	0.533
9D	14,062	--	0.272	0.320	0.364
16D	25,431	0.0289	0.0670	0.0641	0.0707
Naval Air Sta.	36,200	--	--	--	--
(Scheelite?)	20,400	--	--	--	--

TABLE 3.3 PEAK SURFACE PARTICLE VELOCITY IN CM/SEC

Station	Distance (meters)	Vertical			Radial			Transverse			Resultant Vector		
Hardrock		a	d	u	a	d	u	a	d	u	a	d	u
1/2A	954	--	--	--	44.3	--	--	--	--	--	--	--	--
1A	1,500	24.6	26.8	--	24.6	27.5	--	9.26	9.21	--	35.7	30.6	--
		23.5	39.8	--	26.8	31.6	--	--	10.6	--	27.7	42.7	--
2A	3,125	4.38	7.98	--	5.62	4.76	--	2.70	--	--	7.08	8.32	--
3A	4,920	2.74	--	--	4.66	3.69	--	1.87	2.48	--	5.07	3.76	--
1B	1,805	27.9	--	--	24.9	28.5	--	25.5	30.4	--	32.7	33.0	--
2B	3,394	4.28	5.71	--	4.12	--	--	2.30	3.22	--	5.39	5.73	--
3B	4,887	2.11	--	2.00	2.34	--	2.41	1.47	--	1.79	2.42	--	3.12
4B	6,522	1.10	--	1.27	1.47	1.57	2.40	0.926	1.24	1.22	1.71	1.58	2.47
6B	9,668	0.561	--	0.344	0.581	0.599	0.418	0.371	0.480	0.354	0.685	0.672	0.480
1/2C	1,042	55.4	29.8	--	37.2	28.4	--	18.2	--	--	61.1	32.6	--
1C	1,794	18.4	17.9	--	14.5	11.1	--	7.82	5.97	--	19.6	18.7	--
		19.5	21.9	--	13.2	16.8	--	6.72	8.84		22.9	22.5	--
2C	3,392	4.87	4.65	--	7.94	7.50	--	4.19	--	--	8.03	--	--
3 1/2C	5,706	--	--	--	2.71	--	--	--	1.52	--	--	--	--
1D	1,493	36.3	--	--	30.7	33.3	--	11.4	12.5	--	37.7	33.3	--
		37.0	--	--	30.3	28.9	--	--	11.1	--	39.3	28.9	--
East 1	14.430	--	--	0.580	--	--	--	--	--	--	--	--	--
West 1	19,150	--	--	0.236	--	--	--	--	--		--	--	--
Mercury	27,650	--	--	0.131	--	--	--	--	--	--	--	--	--
North 2	29,000	--	--	0.119	--	--	--	--	--	--	--	--	--
East 2	39,900	--	--	0.113	--	--	--	--	--	--	--	--	--
Gabbs Mine	55,400	--	--	--	--	--	--	--	--	--	--	--	--
(Scheelite?)	20,400	--	--	--	--	--	--	--	--	--	--	--	--

TABLE 3.3 (cont.)

Station	Distance (meters)	Vertical			Radial			Transverse			Resultant Vector		
Alluvium		a	d	u	a	d	u	a	d	u	a	d	u
4 1/2A	7,147	3.47	5.50	--	7.55	8.30	--	3.77	4.35	--	7.92	8.63	--
8A	12,820	--	--	--	1.50	1.53	--	1.38	1.71	--	--	--	--
12A	18,890	0.802	--	--	0.876	--	--	1.22	--	--	1.22	--	--
3D	4,720	9.67	9.92	--	6.19	6.63	--	4.68	4.70	--	9.84	9.91	--
4 1/2D	6,921	1.11	--	--	3.57	4.44	--	3.18	3.44	--	3.77	4.44	--
9D	14,062	--	--	--	--	2.14	--	1.43	1.44	--	--	2.28	--
16D	25,431	--	0.326	--	0.723	0.801	--	0.757	0.855	--	0.855	0.901	--
Naval Air Sta.	36,200	--	--	--	--	--	--	--	--	--	--	--	--
(Scheelite?)	20,400	--	--	--	--	--	--	--	--	--	--	--	--

[a] Velocity derived from accelerometers.
[d] Velocity derived from displacement meters.
[u] Velocity from velocity meters.

TABLE 3.4 STATIONS USED IN COMPARISON OF DATA MEASURED PARALLEL AND PERPENDICULAR TO DIRECTION OF MAJOR FAULTING

Orientation	Station
Parallel	½A 1A 2A 3A ½C 1C 2C 3½C
Perpendicular	1B 2B 3B 4B 6B 1D

TABLE 3.5 RATIO OF $\frac{u^2}{ad}$

Station	Component	a Acceleration cm/sec^2	d Displacement cm	u Velocity cm/sec	$\frac{u^2}{ad}$
3B	Z	77.3	-	2.00	-
	R	45.2	-	2.41	-
	T	62.5	-	1.79	-
	vector	83.3	-	3.12	-
4B	Z	30.8	-	1.27	-
	R	36.4	.232	2.40	.68
	T	30.6	.124	1.22	.39
	vector	41.3	.239	2.47	.62
6B	Z	20.6	-	.344	-
	R	11.8	.127	.418	.12
	T	9.72	.0766	.354	.17
	vector	22.1	.138	.480	.076

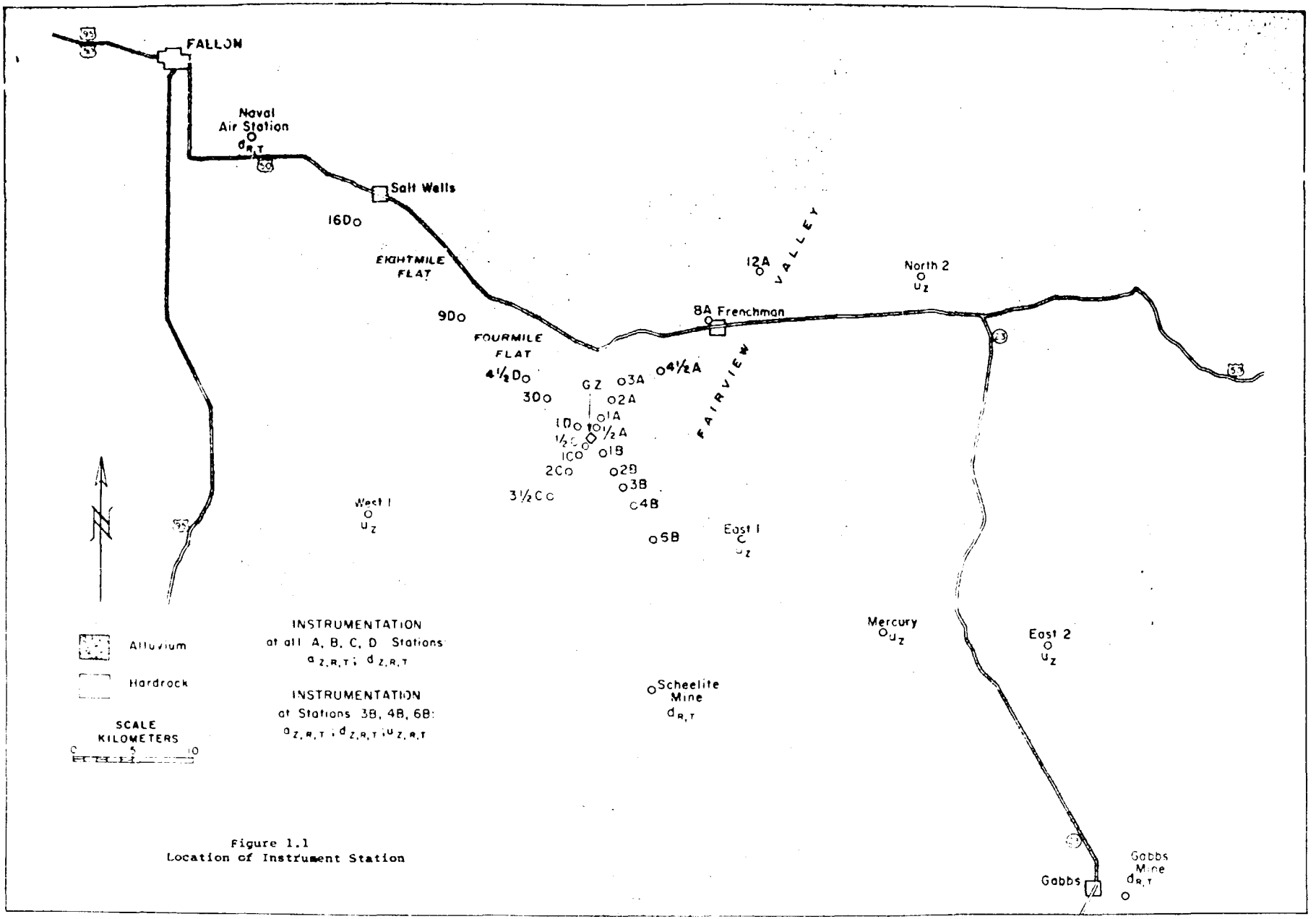

Figure 1.1
Location of Instrument Station

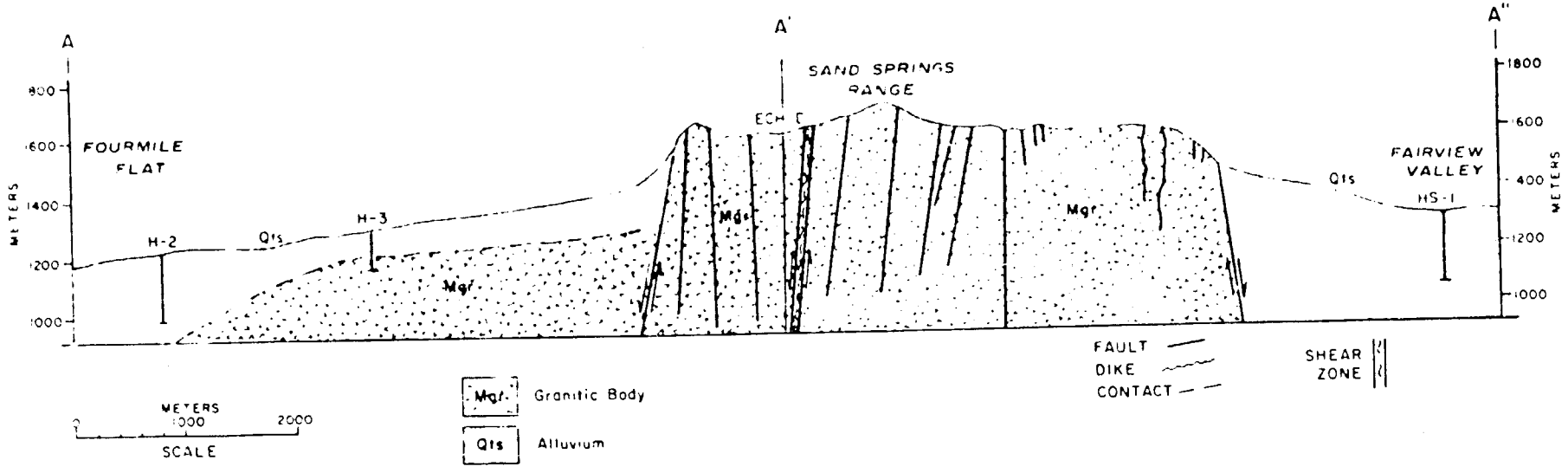

Figure 1.2
Cross Section A-A'-A"

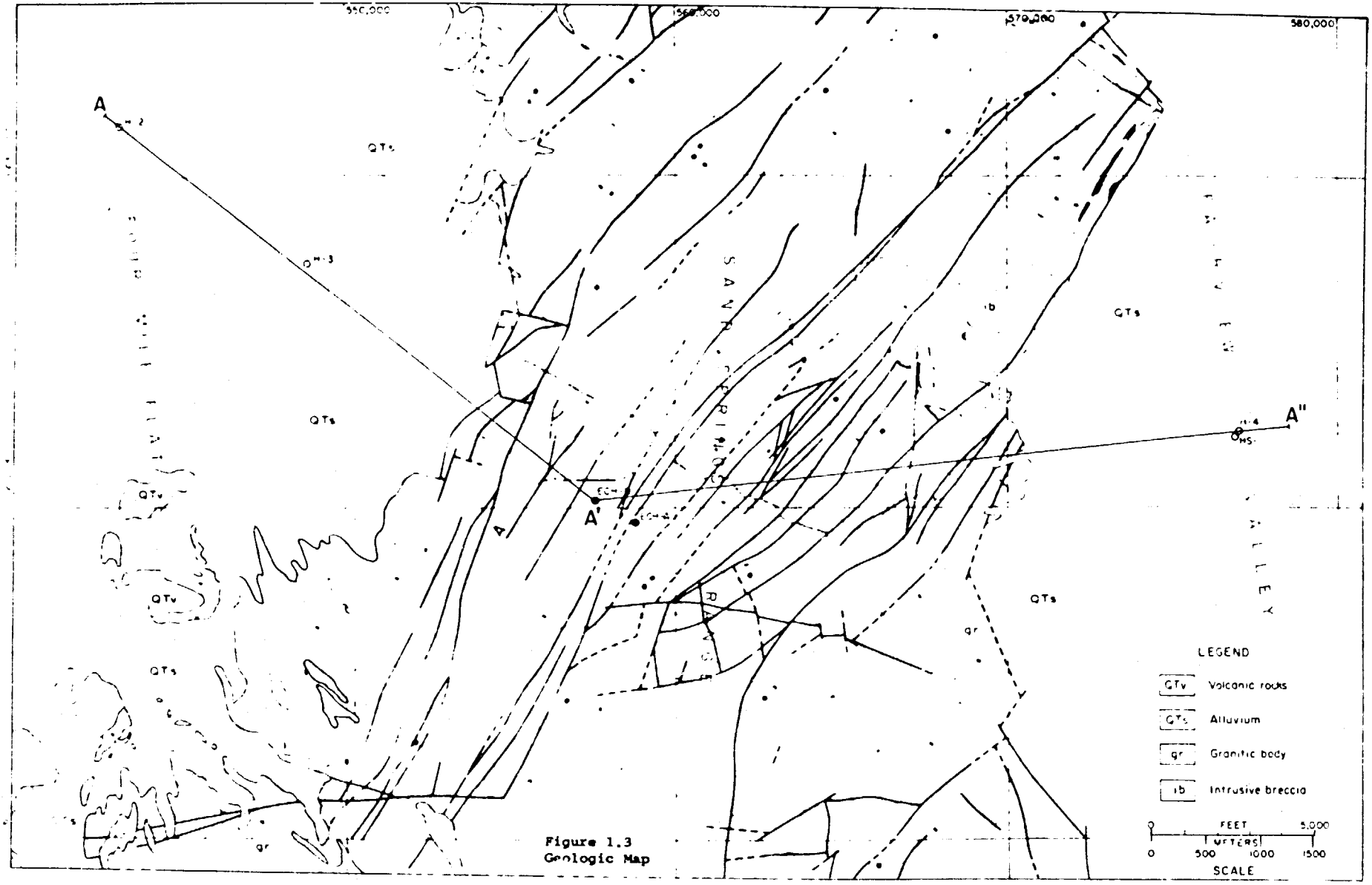

Figure 1.3
Geologic Map

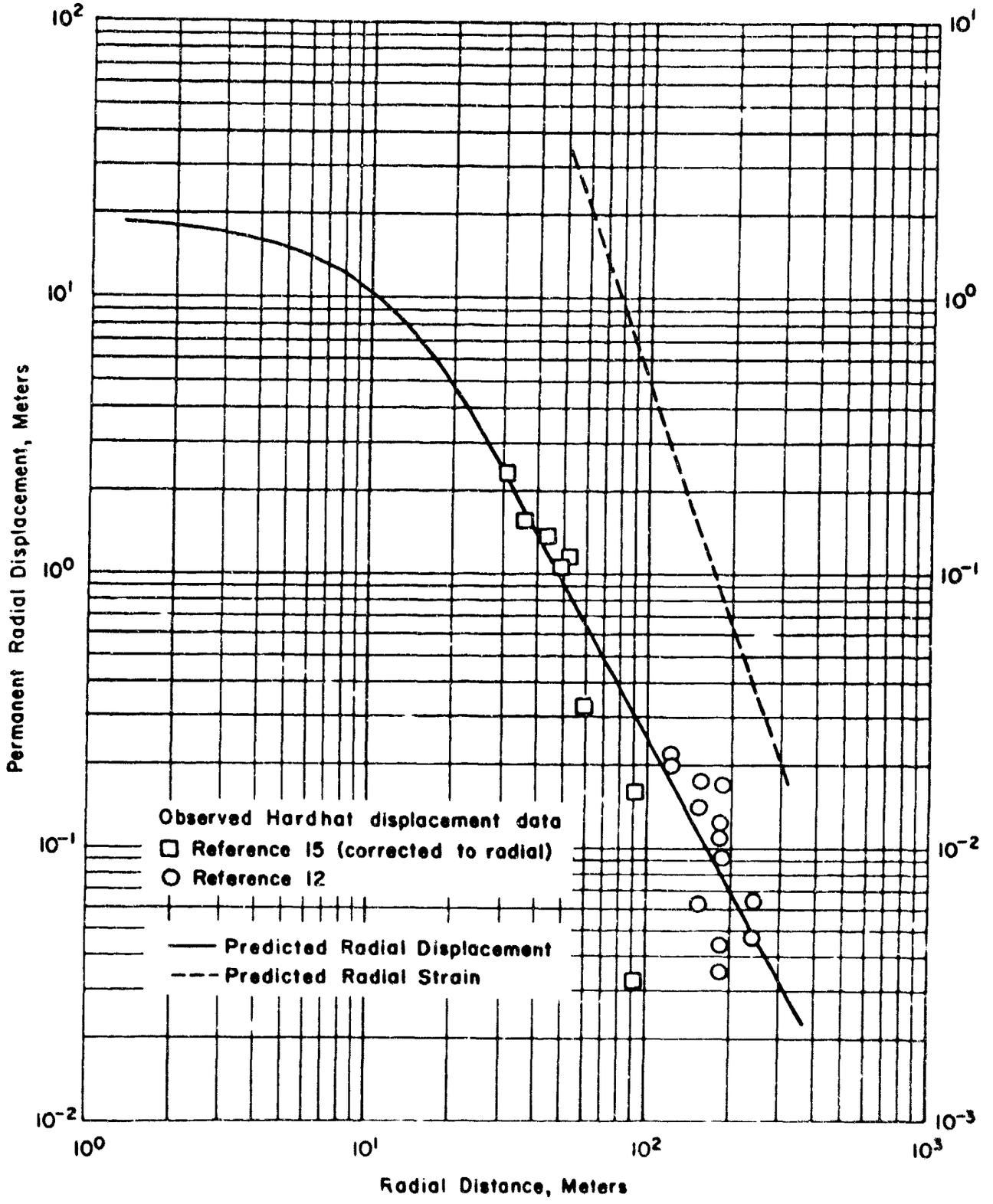

Figure 2.1 Predicted and Observed Permanent Radial Displacement and Predicted Strain for the Hardhat Event

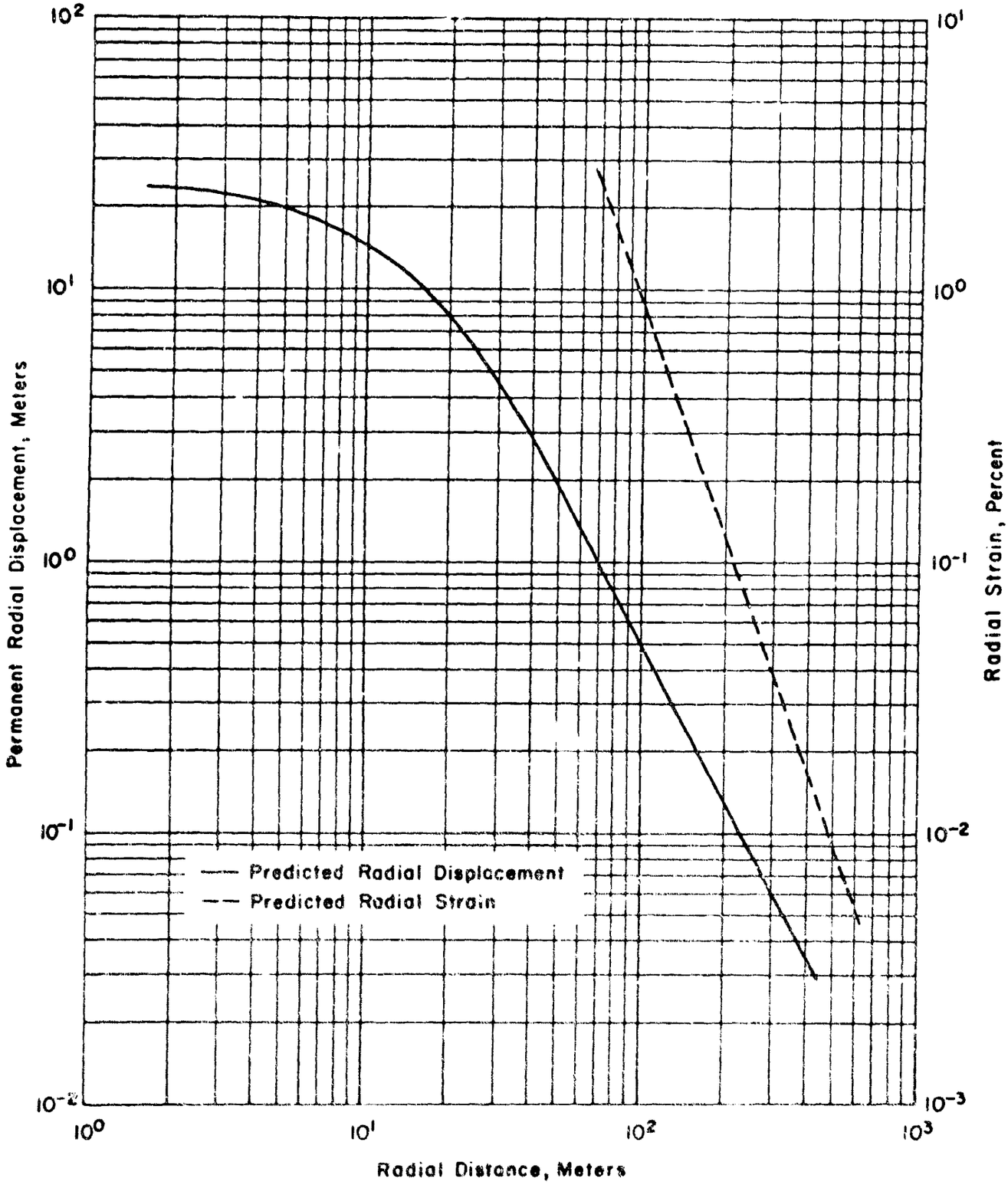

Figure 2.2 Predicted Strain and Permanent Radial Displacement for the Shoal Event

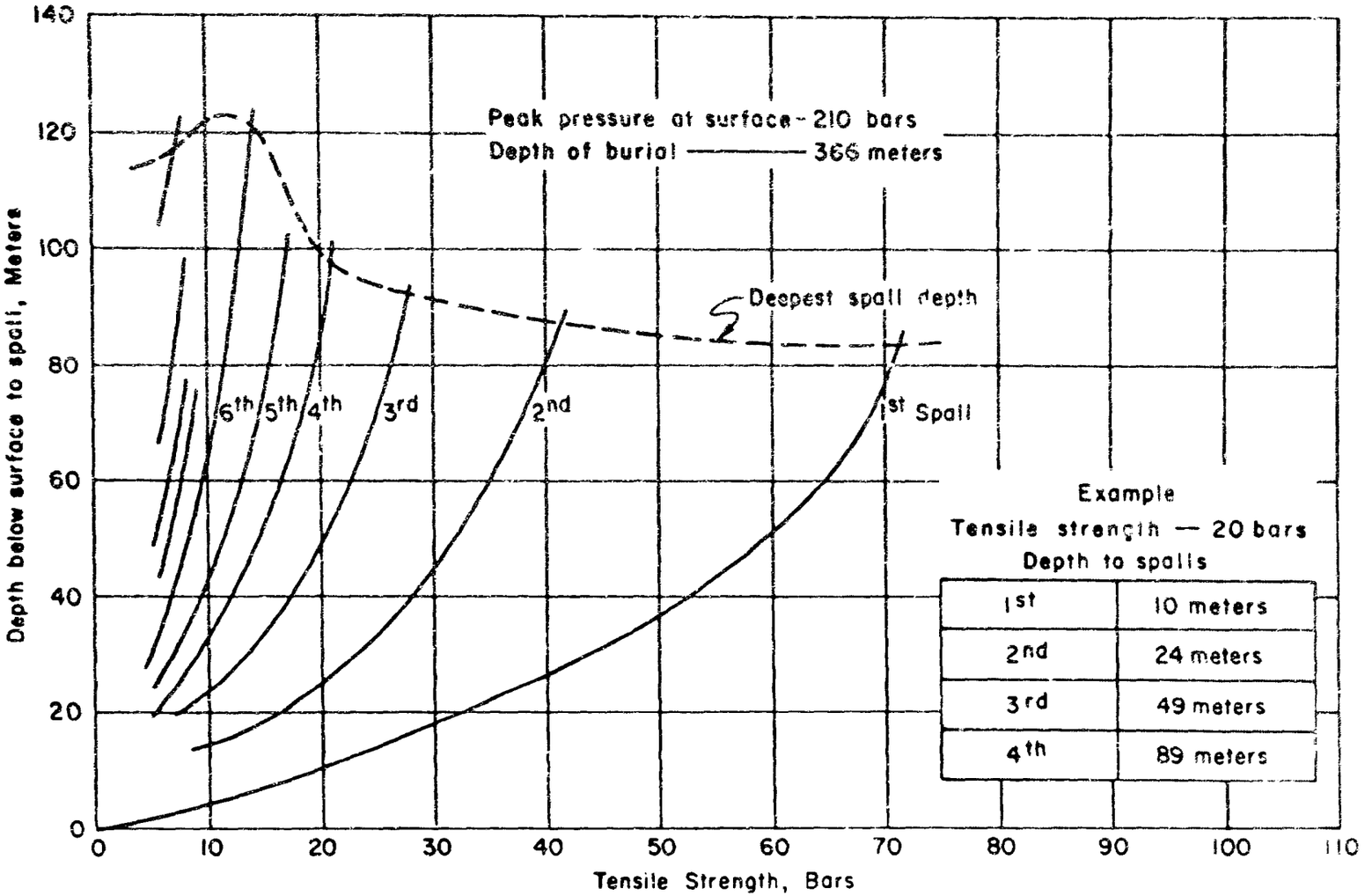

Figure 2.3 Spall Depth as a Functio
of Tensile Strength for Shoal Granite

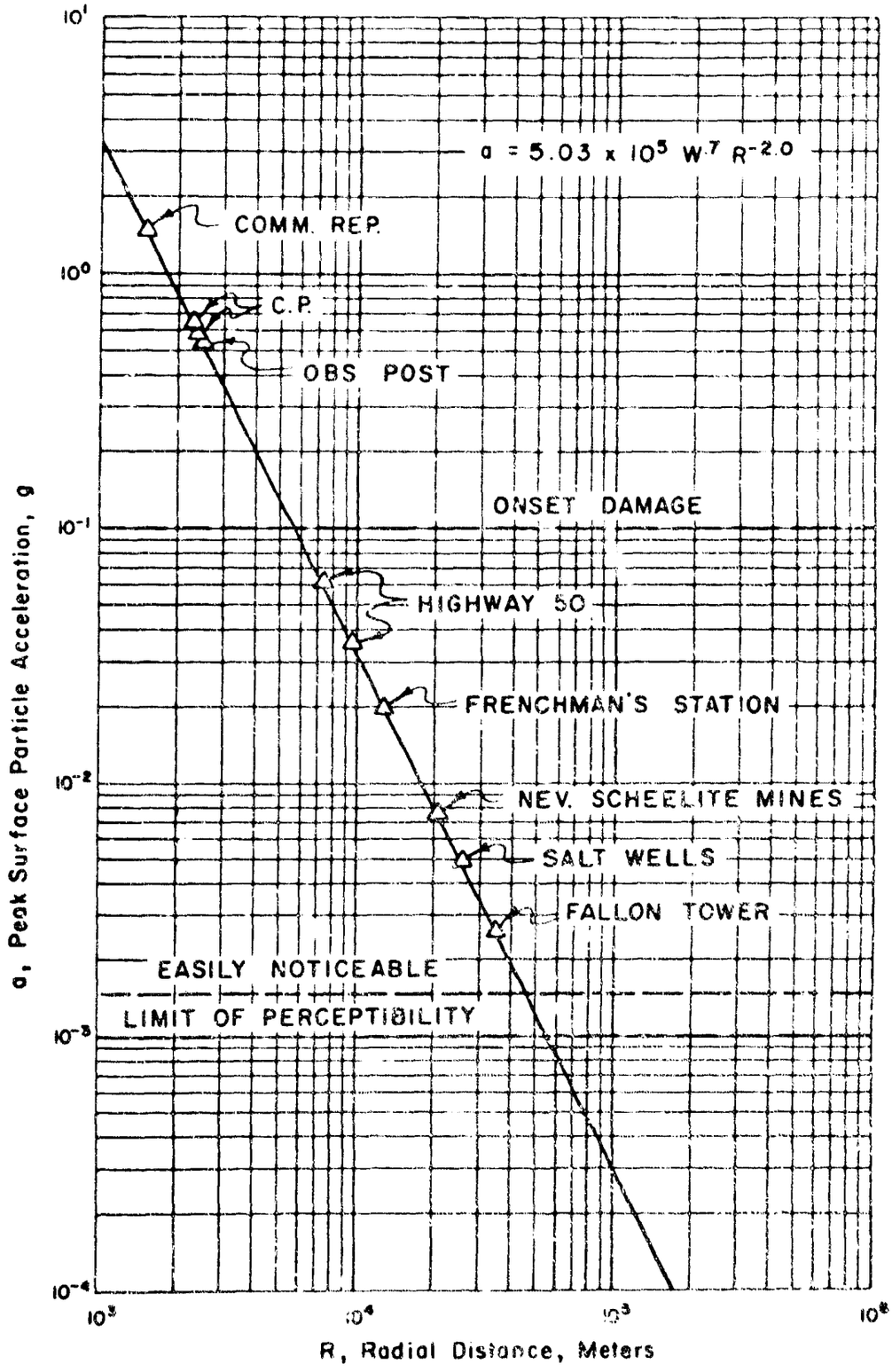

Figure 2.4 Predicted Peak Surface Particle Acceleration as a Function of Horizontal Distance, Shoal Event

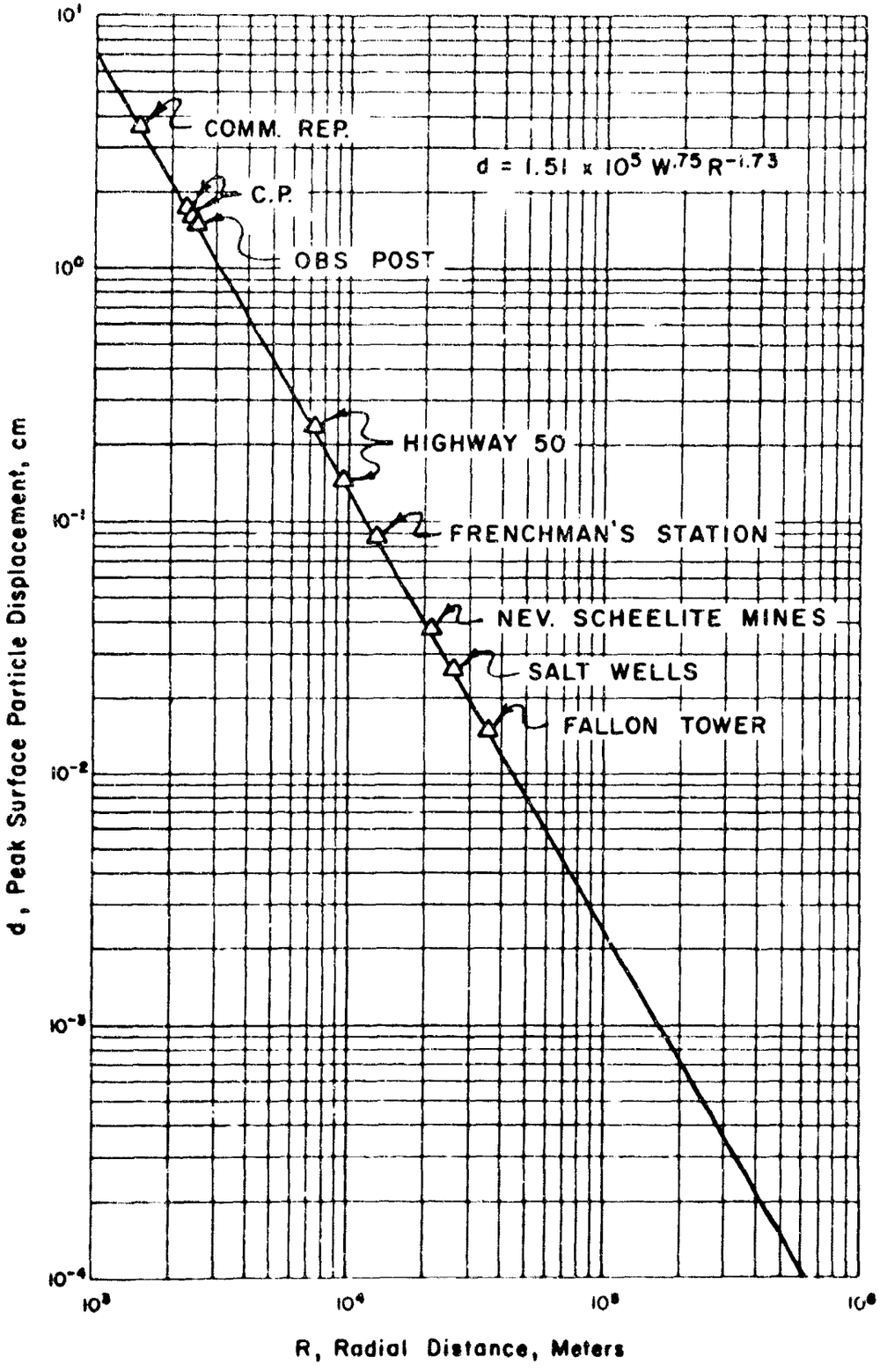

Figure 2.5 Predicted Peak Surface Particle Displacement as a Function of Horizontal Distance, Shoal Event

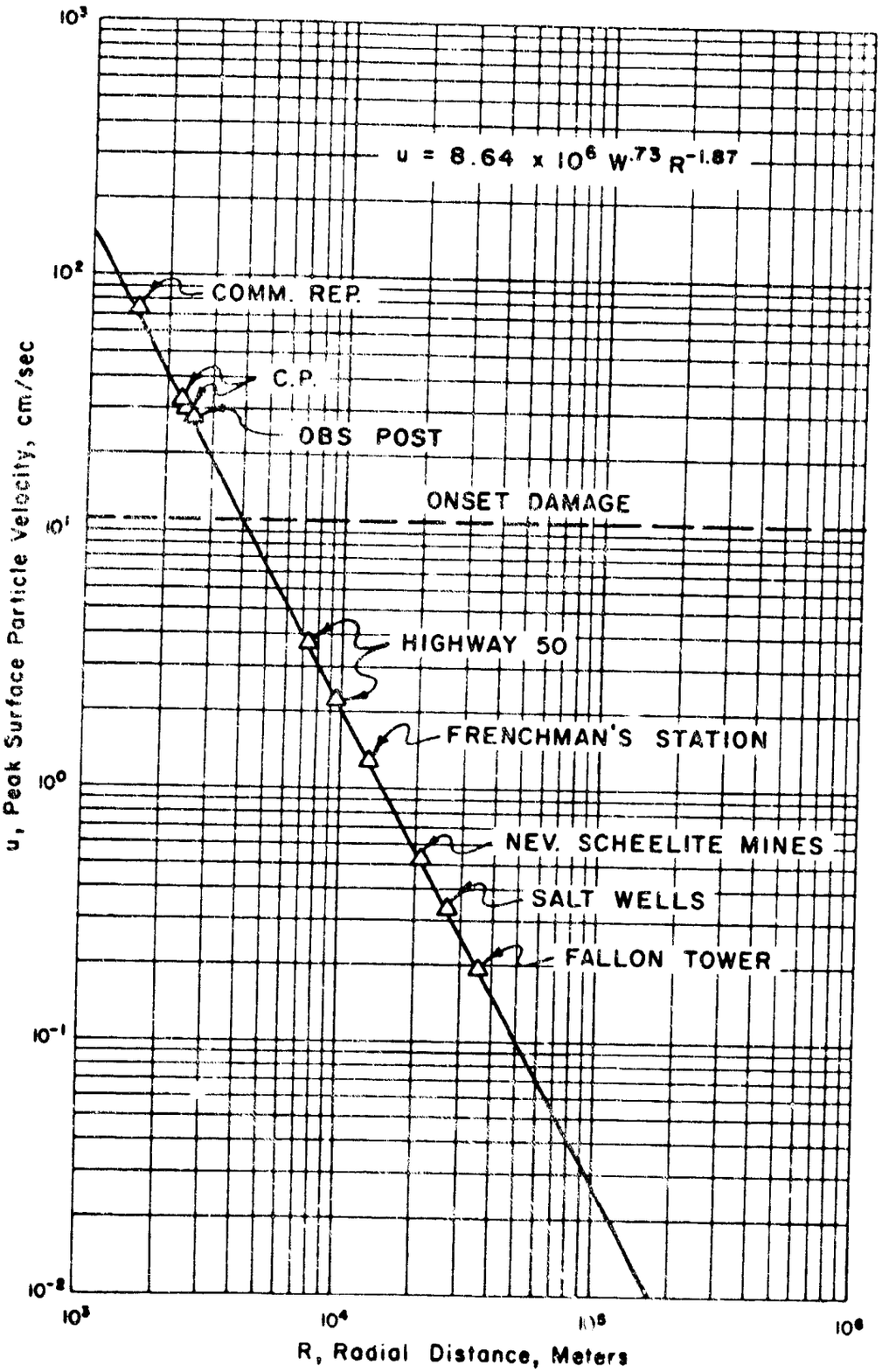

Figure 2.6 Predicted Peak Surface Particle Velocity as a Function of Horizontal Distance, Shoal Event

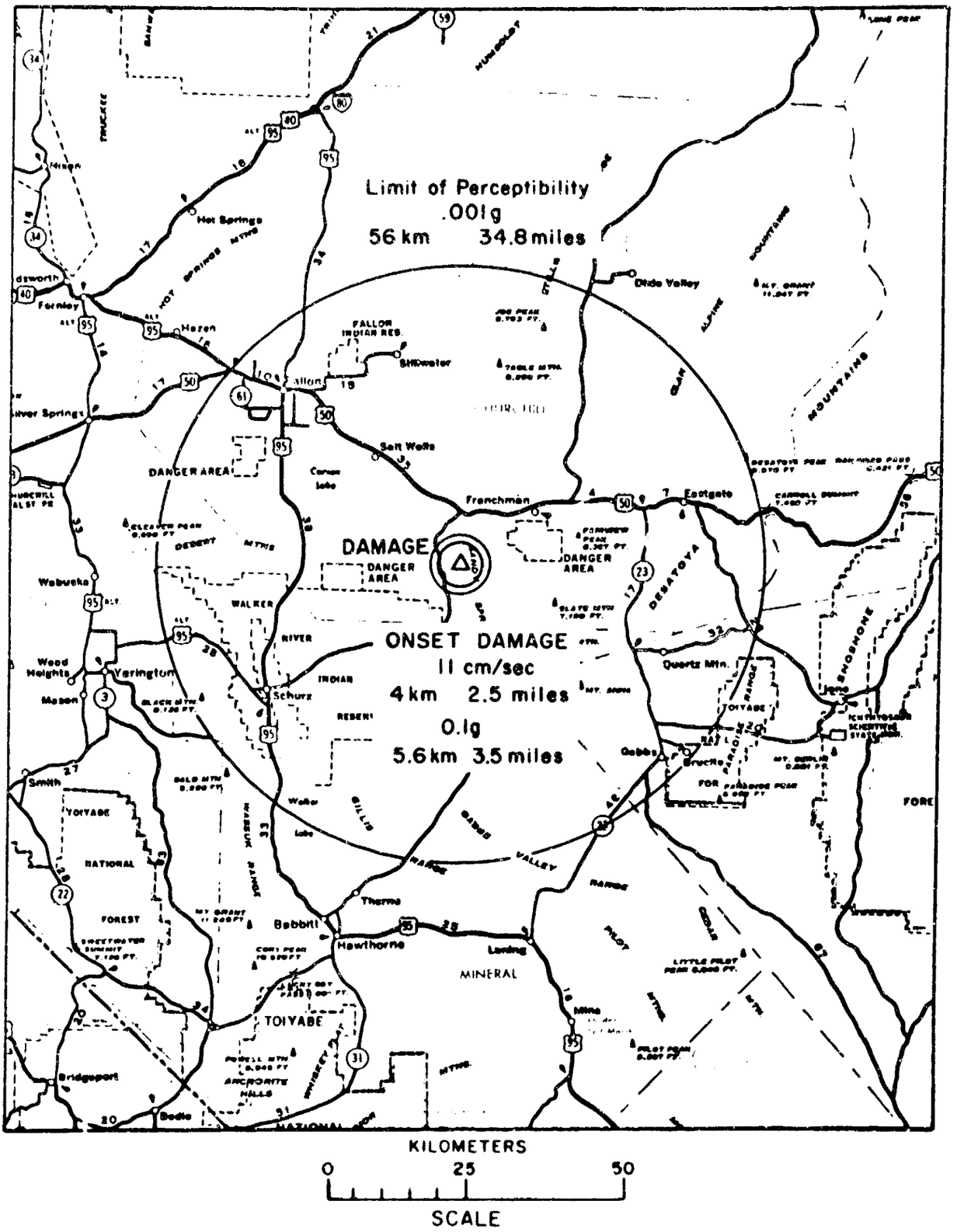

Figure 2.7 Area Map Showing Predicted Distances to Significant Ground Motions

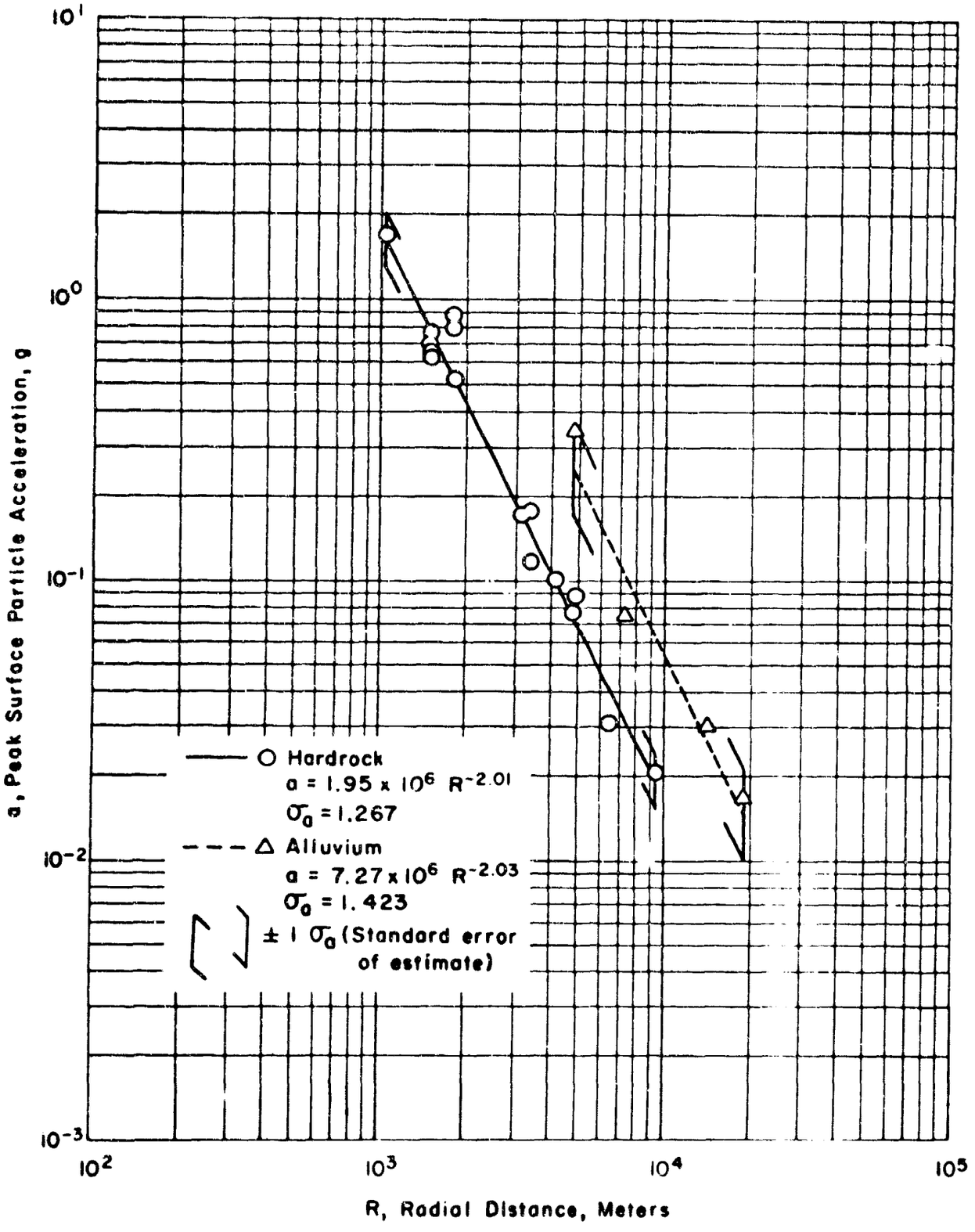

Figure 3.1 Vertical Component of Acceleration

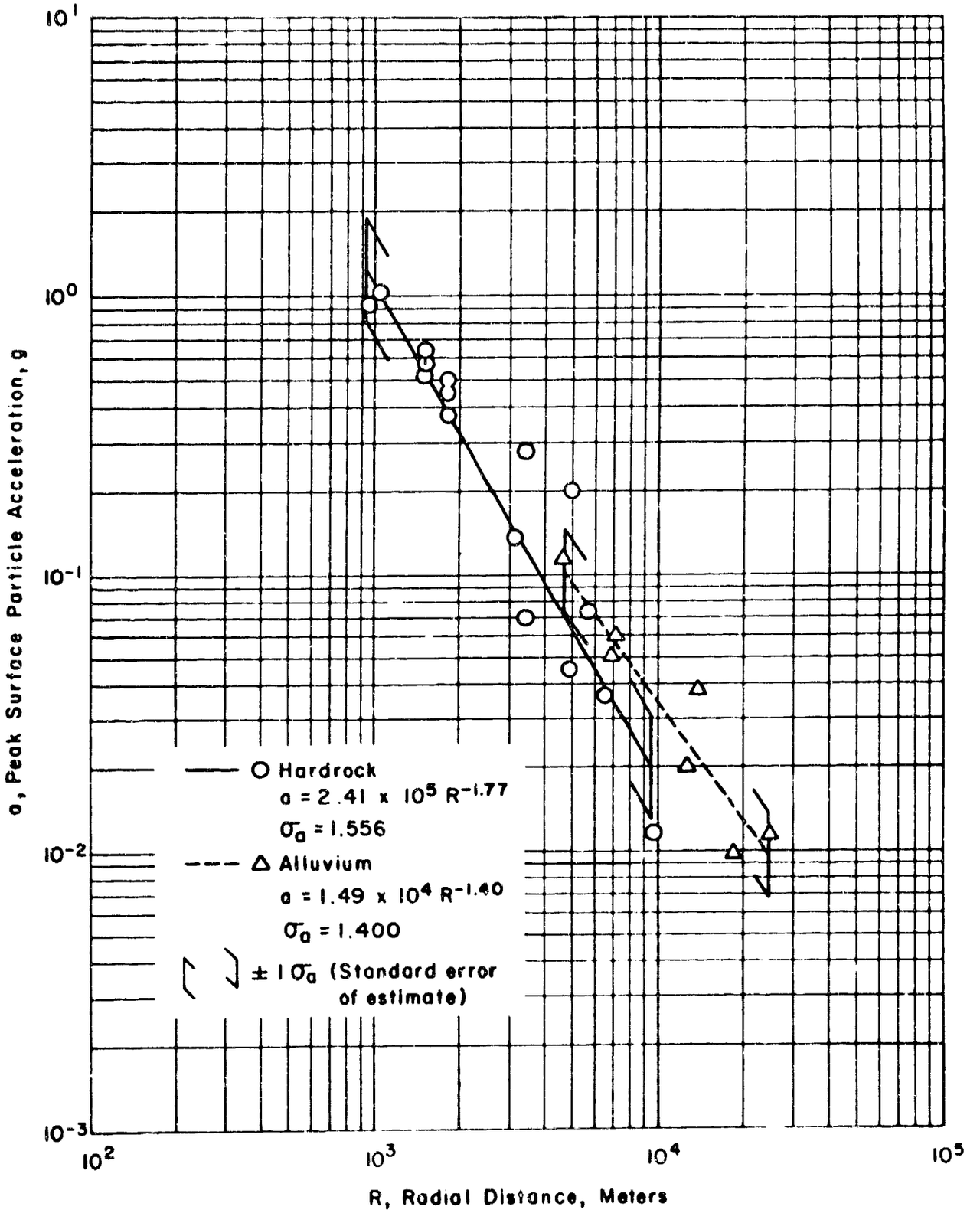

Figure 3.2 Radial Component of Acceleration

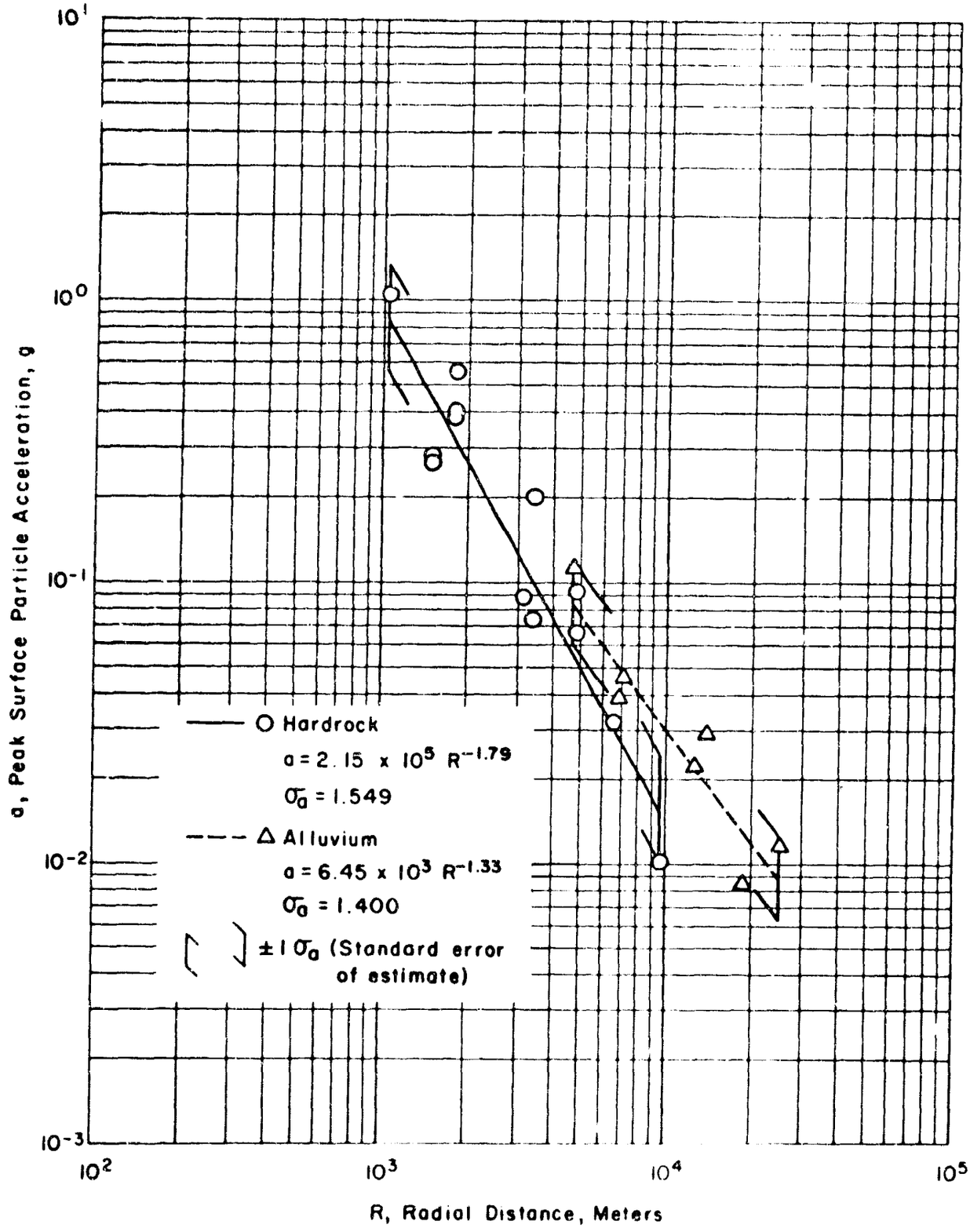

Figure 3.3 Transverse Component of Acceleration

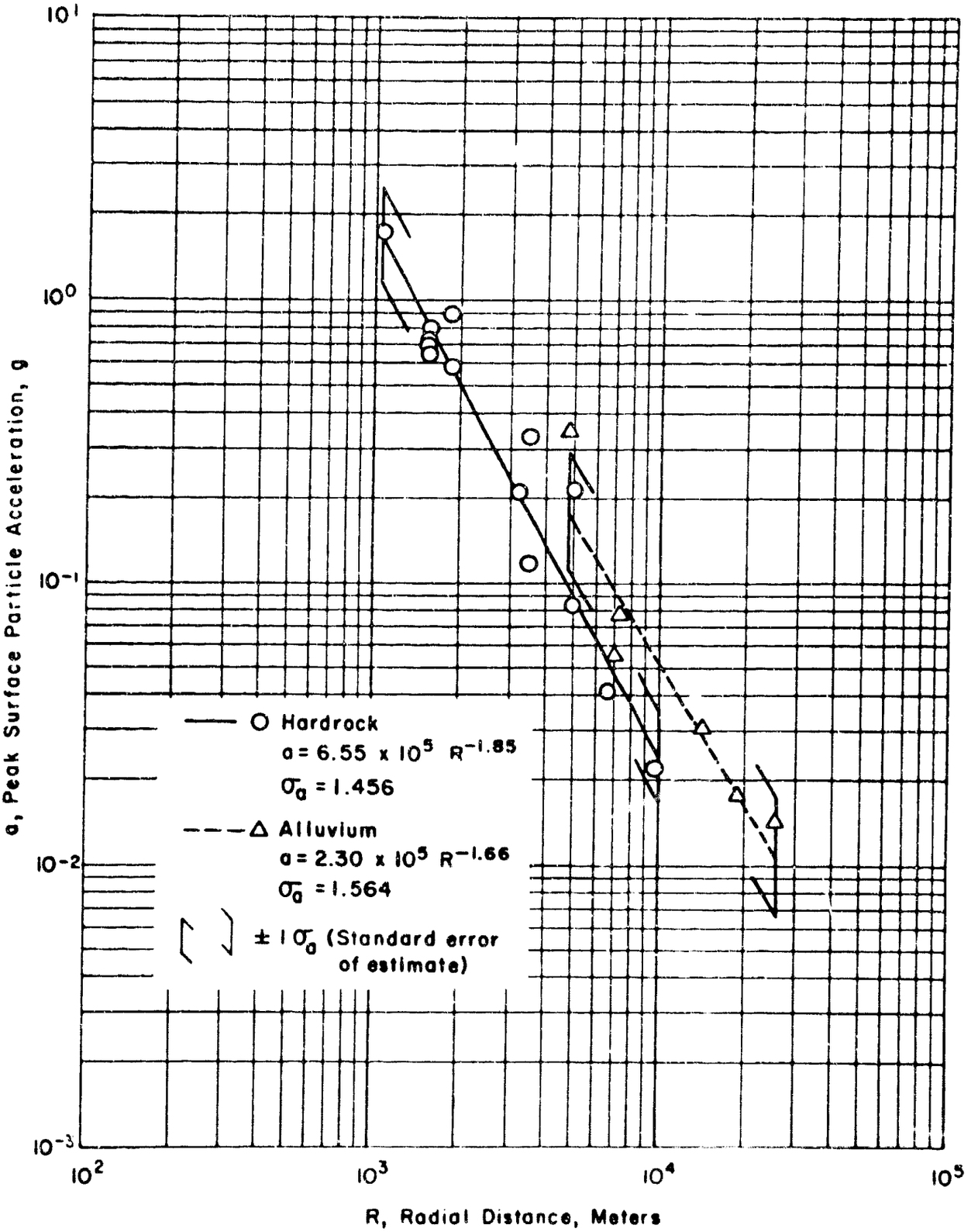

Figure 3.4 Resultant Vector of Acceleration

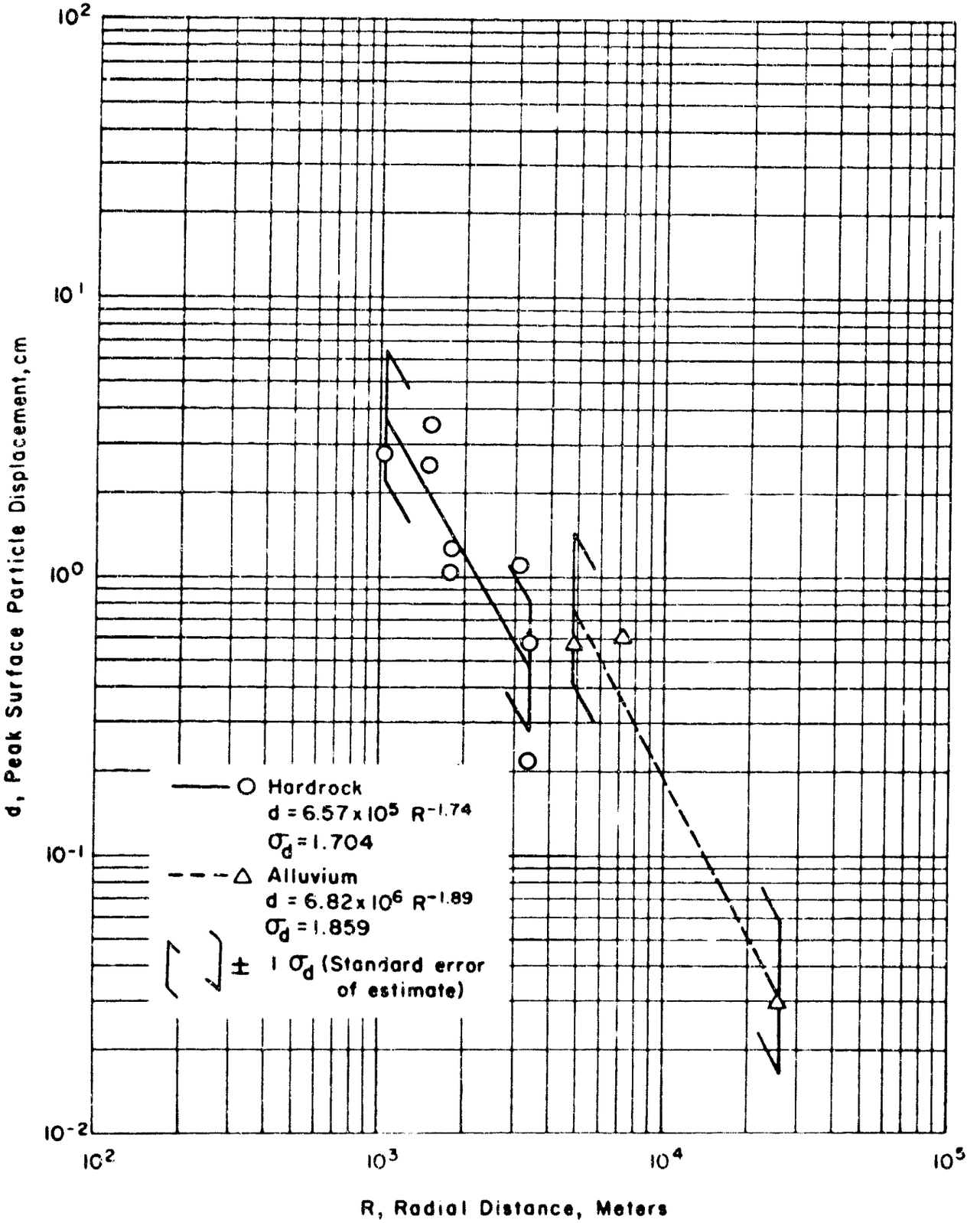

Figure 3.5 Vertical Component of Displacement

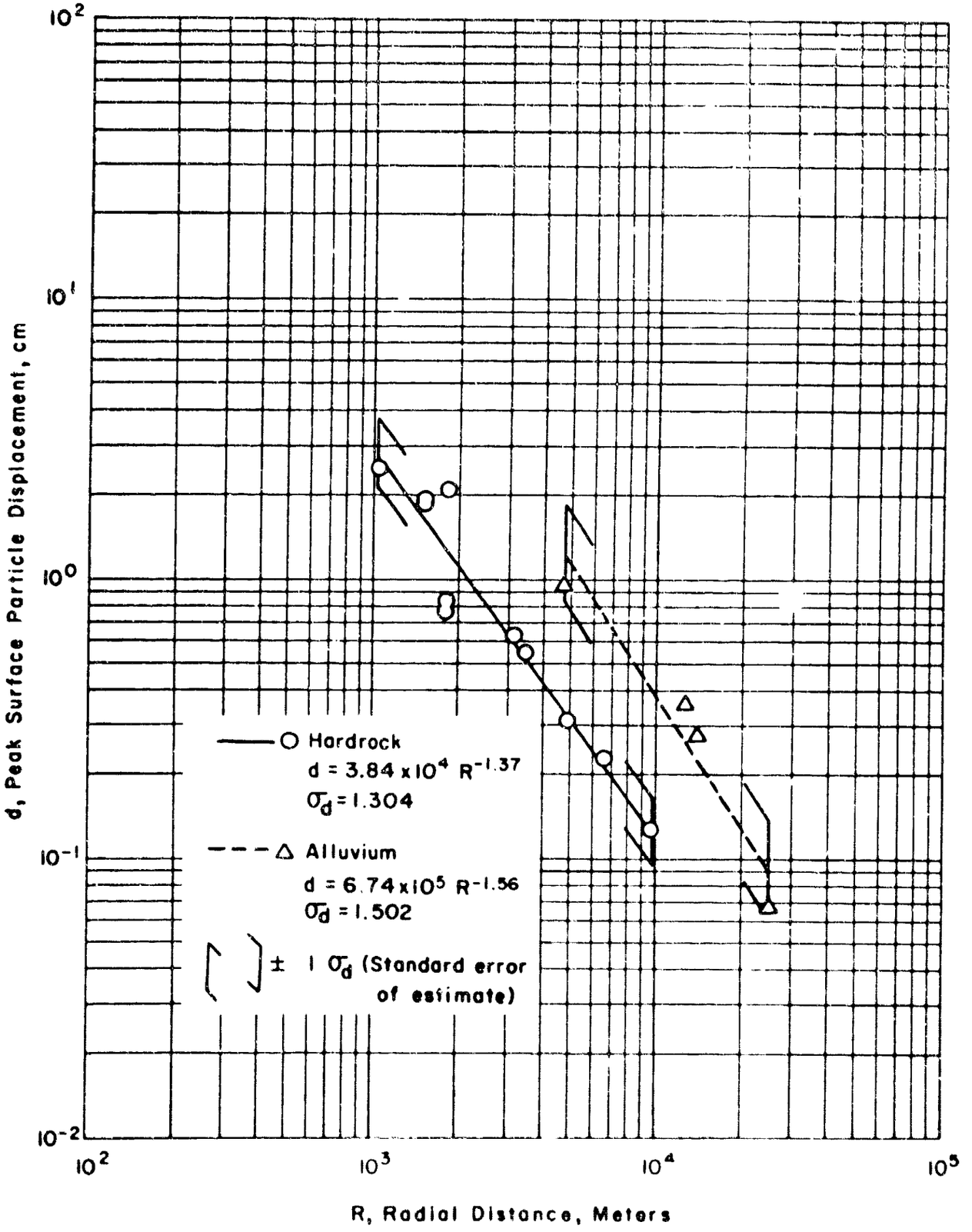

Figure 3.6 Radial Component of Displacement

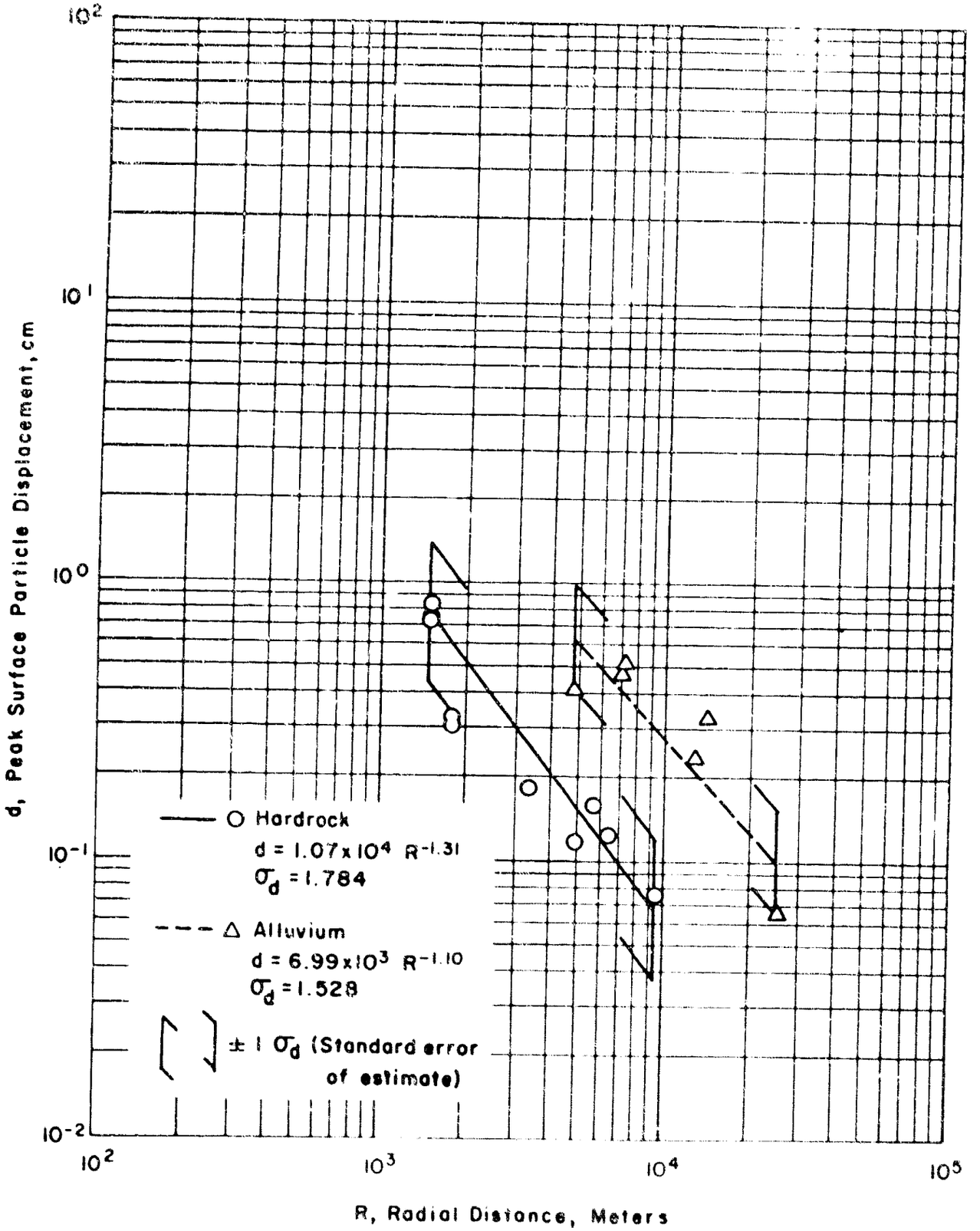

Figure 3.7 Transverse Component of Displacement

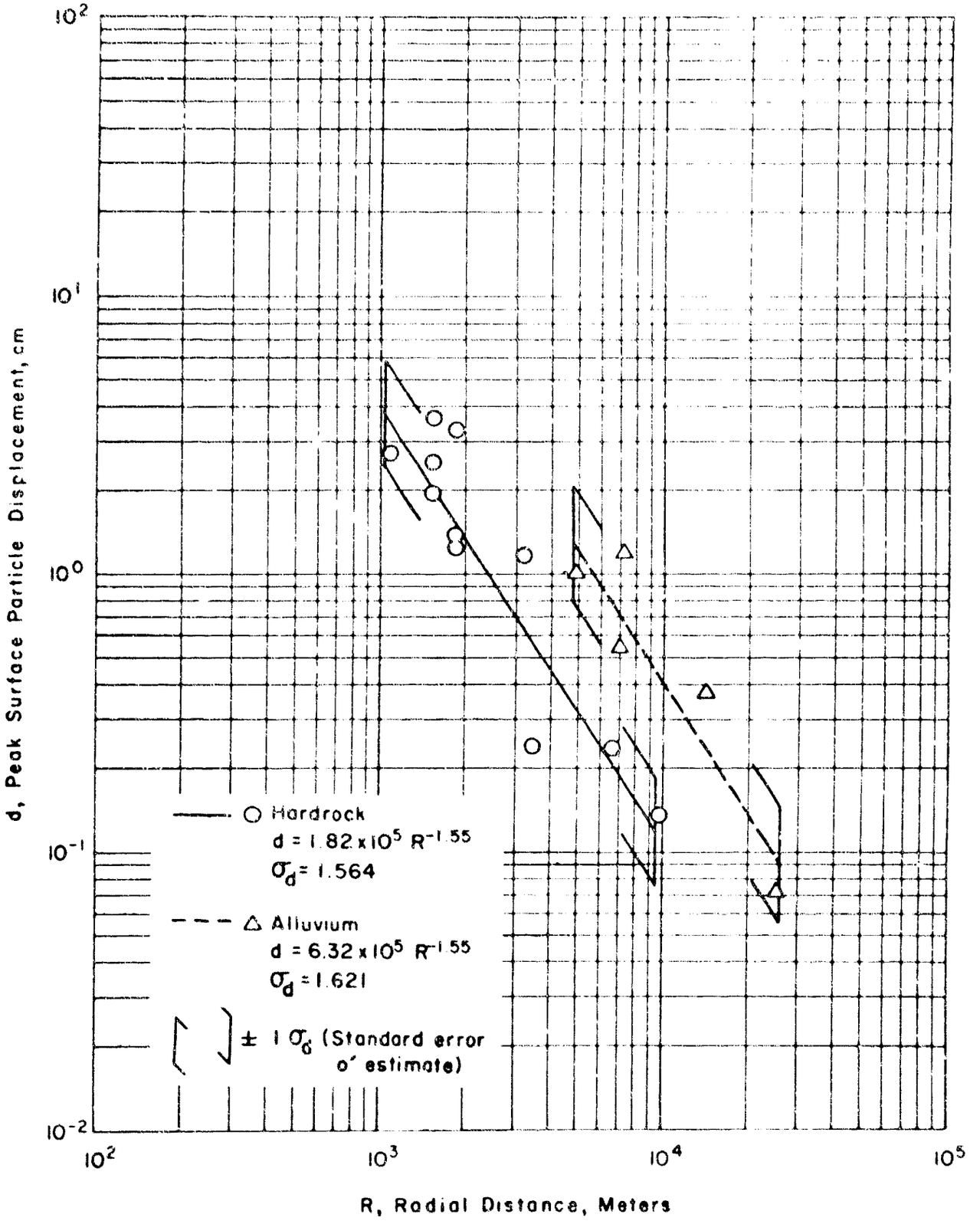

Figure 3.8 Resultant Vector of Displacement

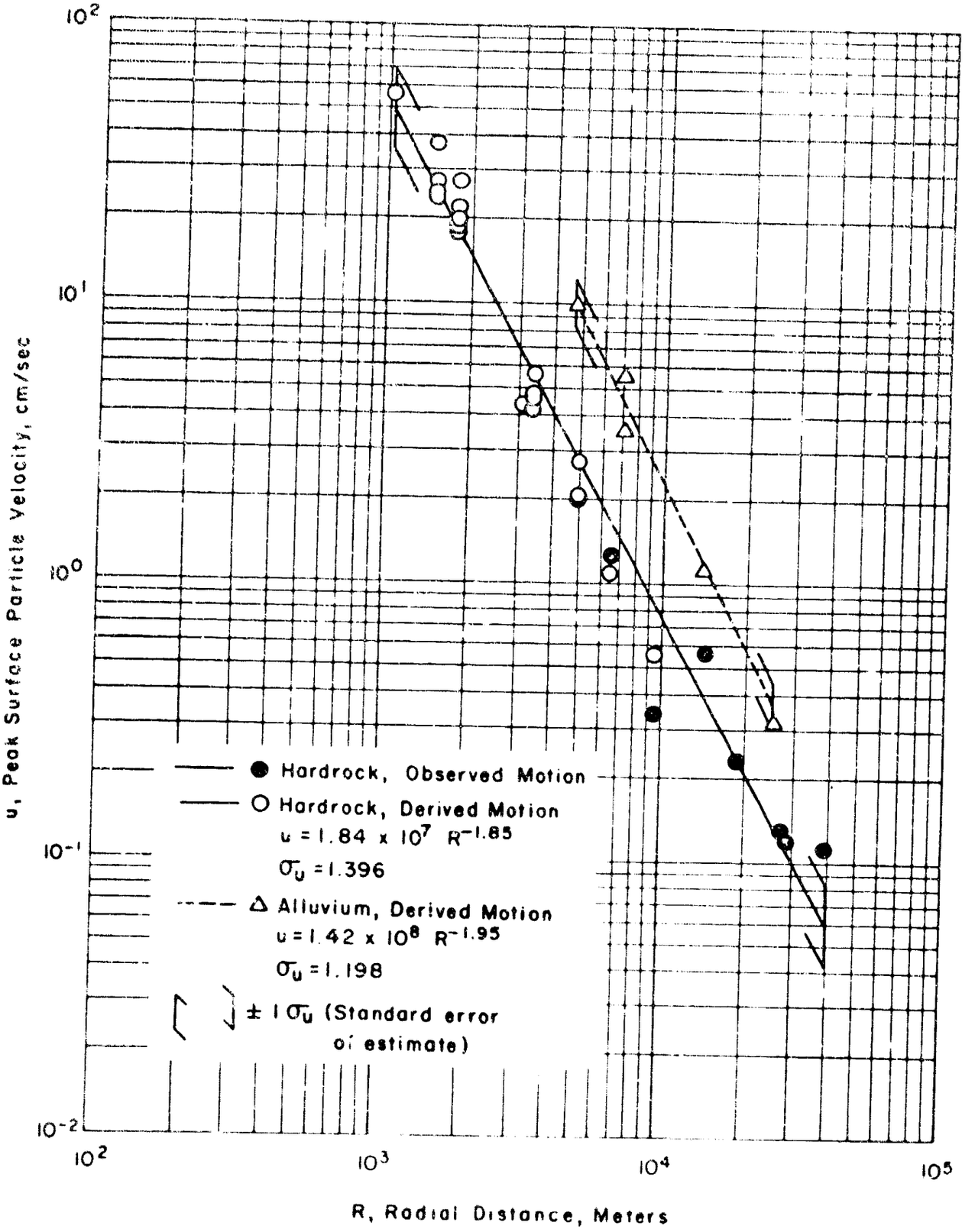

Figure 3.9 Vertical Component of Velocity

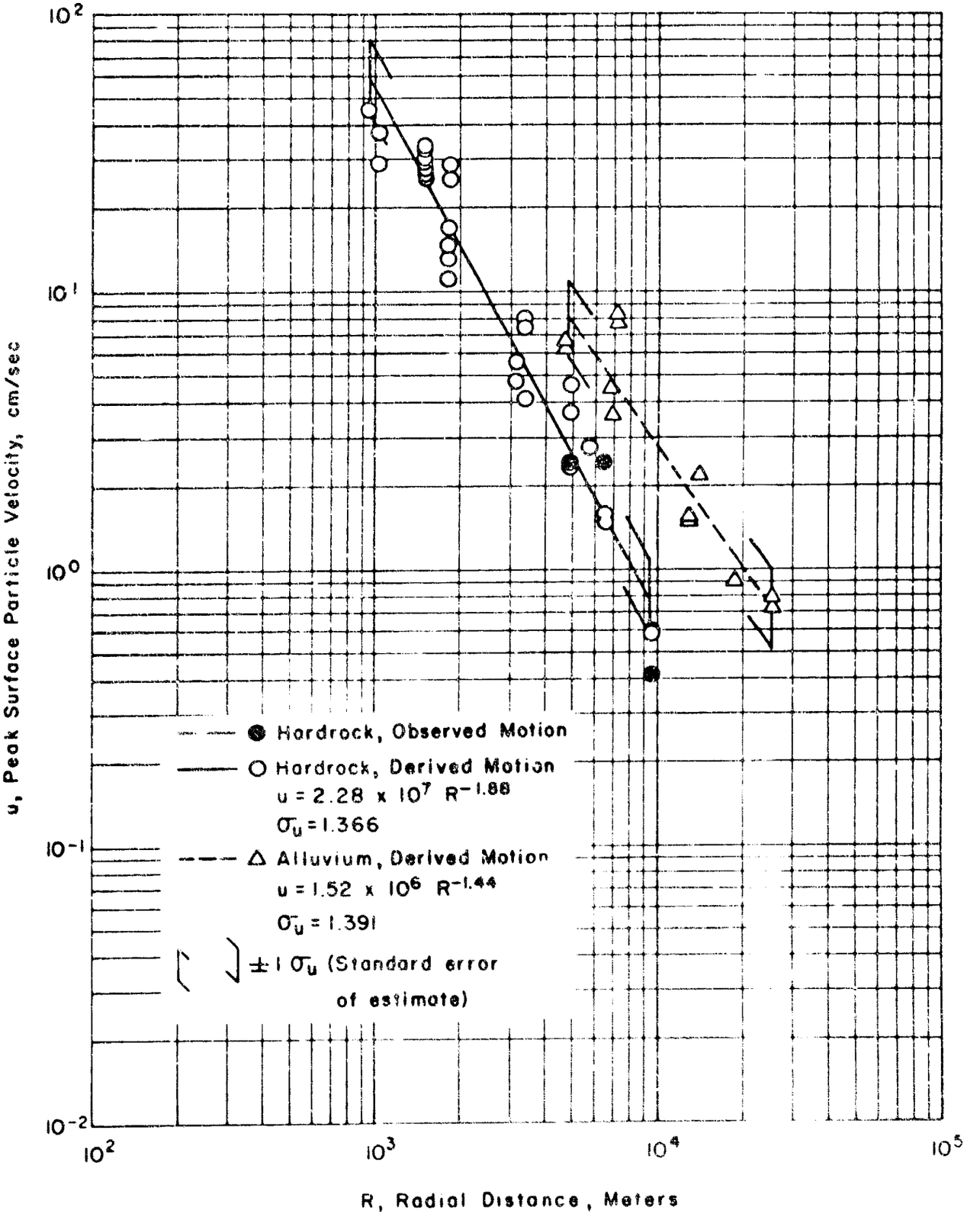

Figure 3.10 Radial Component of Velocity

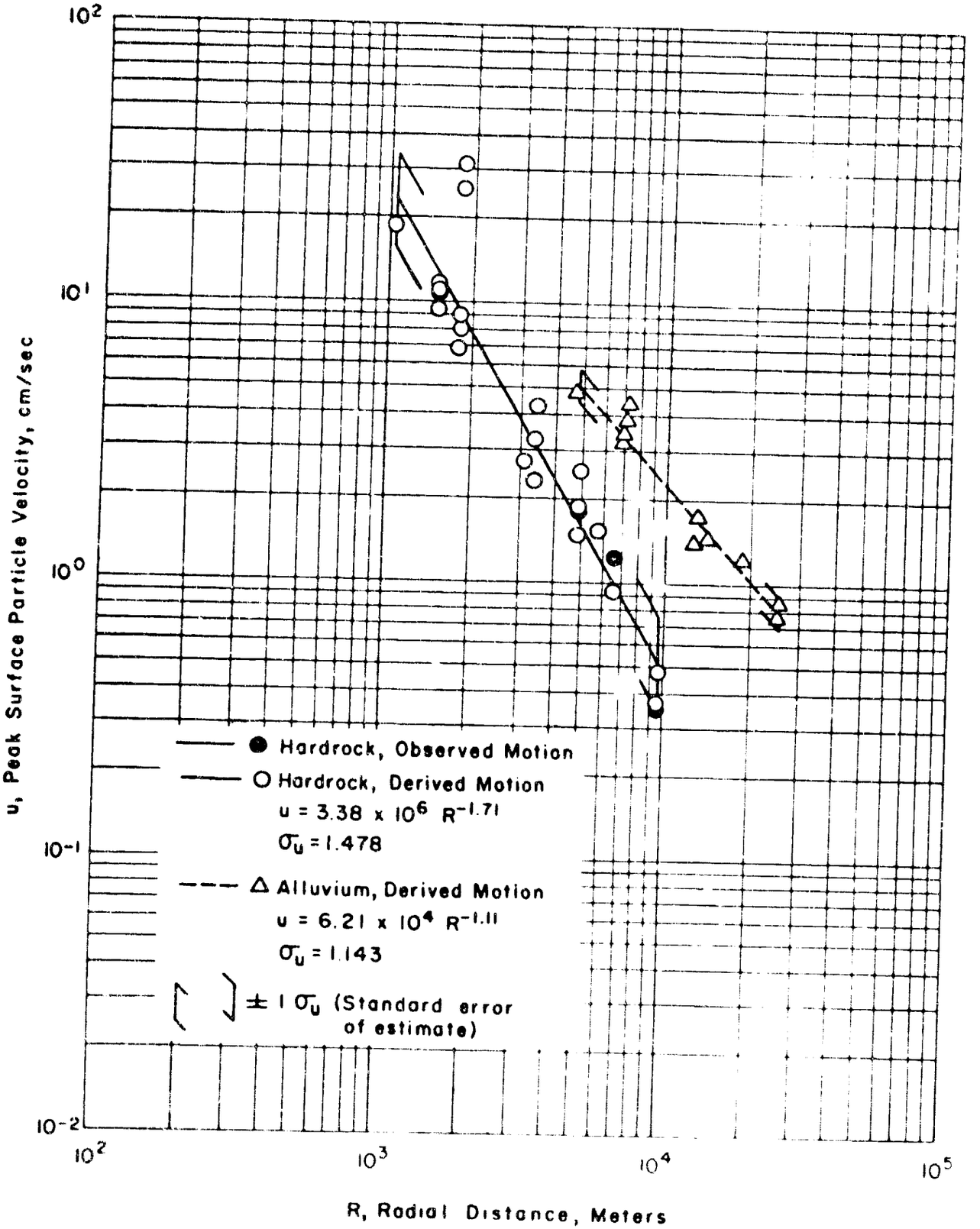

Figure 3.11 Transverse Component of Velocity

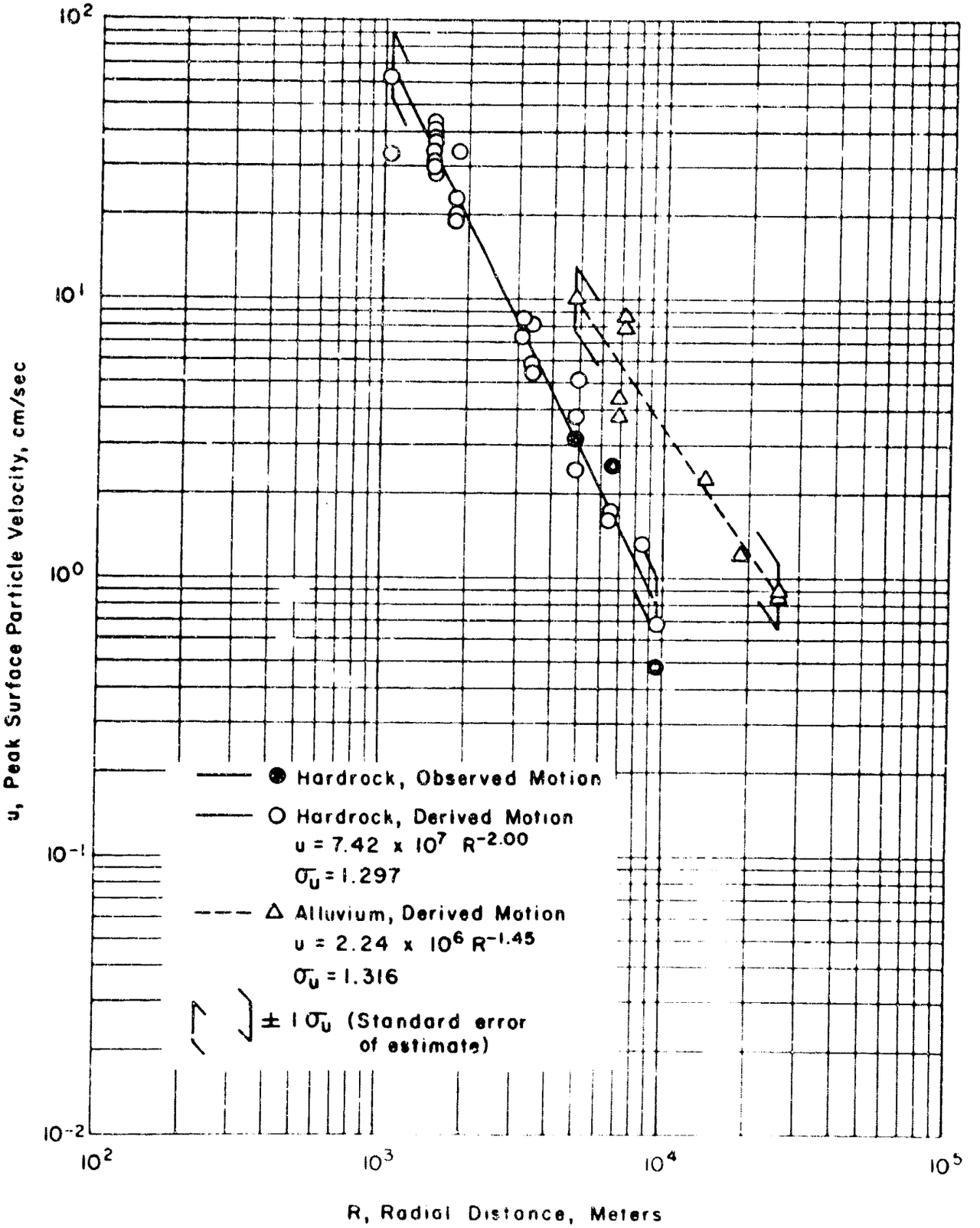

Figure 3.12 Resultant Vector of Velocity

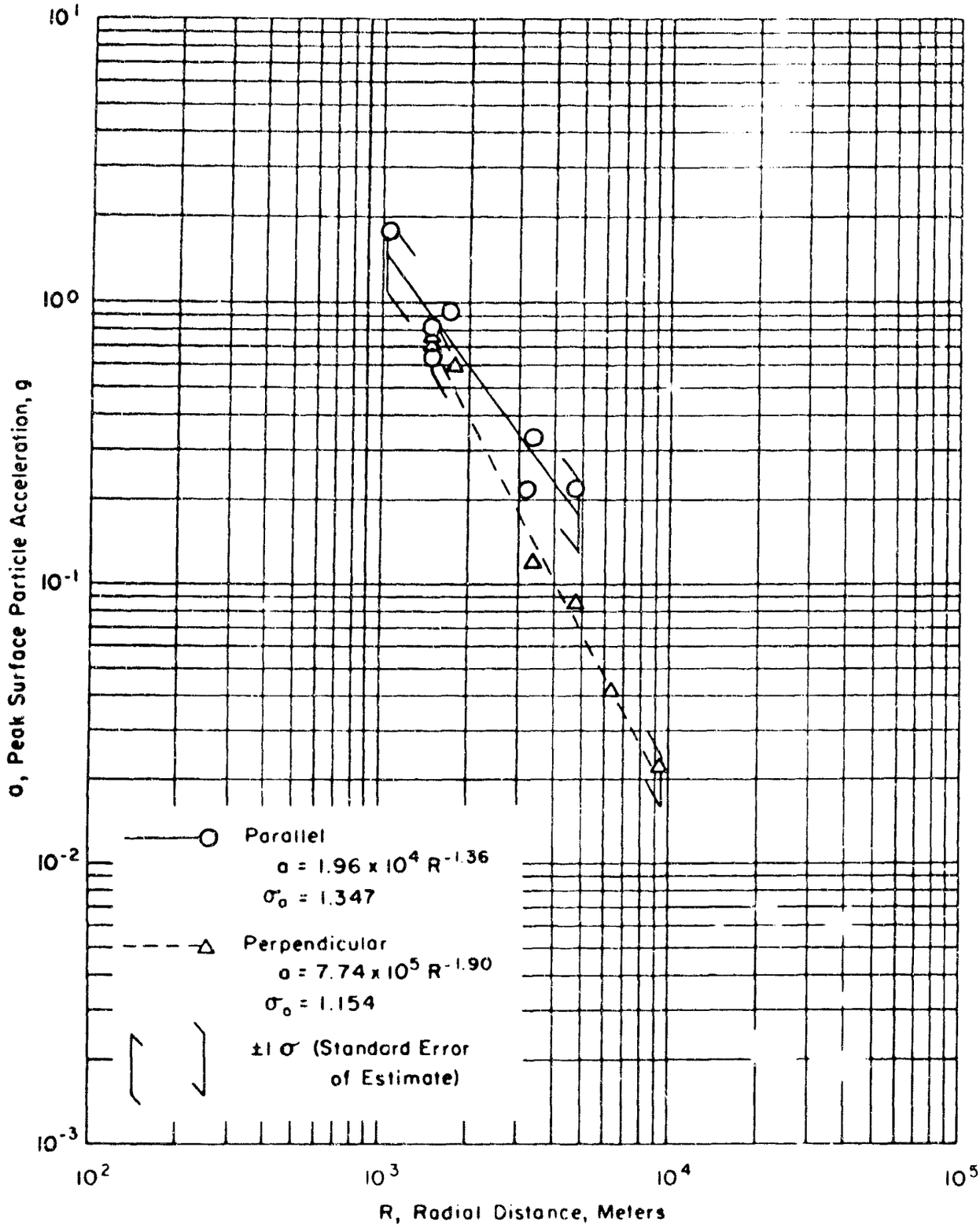

Figure 3.13 Comparison of Resultant Vector of Acceleration Measured Parallel and Perpendicular to Major Fault Trend

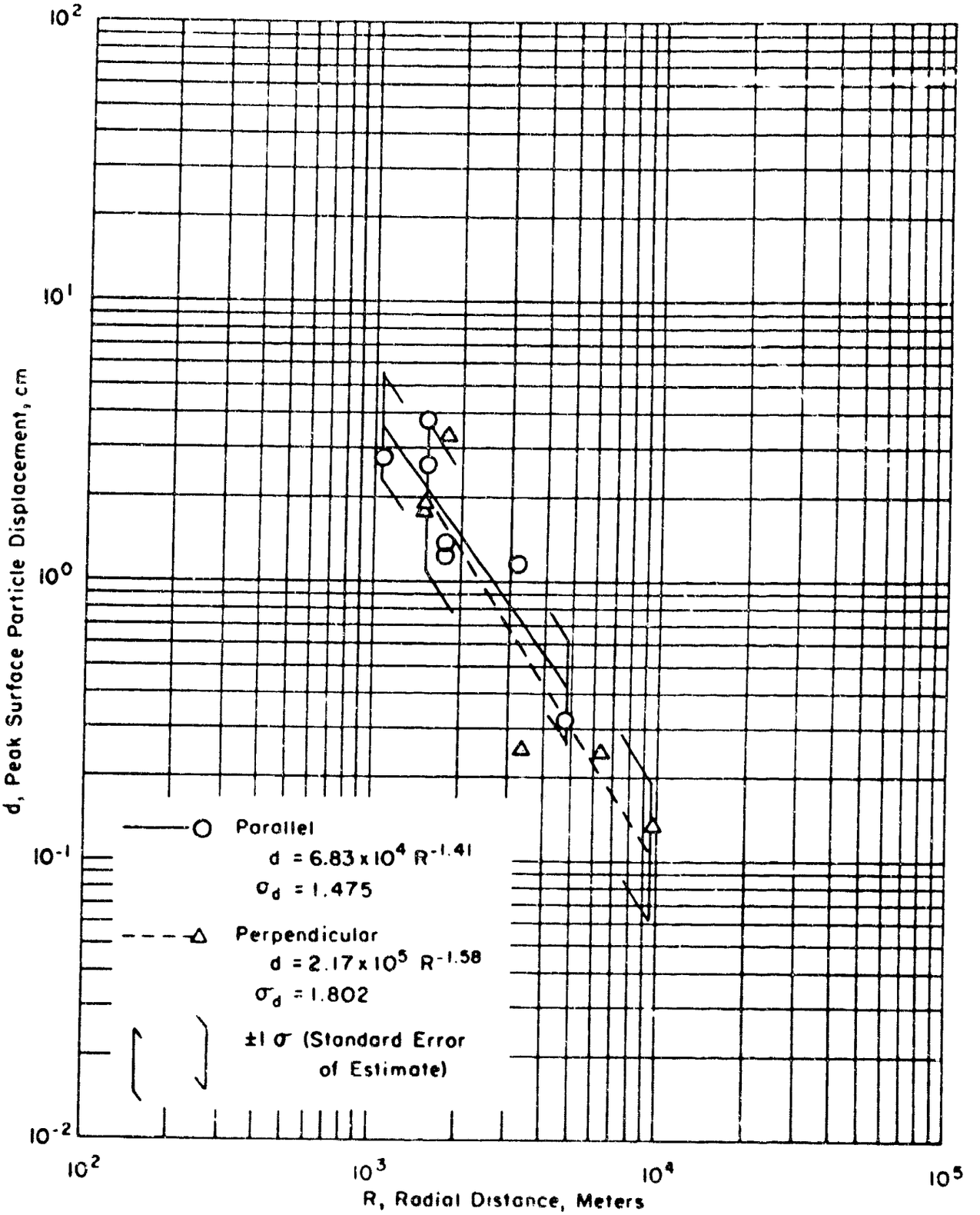

Figure 3.14 Comparison of Resultant Vector of Displacement Measured Parallel and Perpendicular to Major Fault Trend

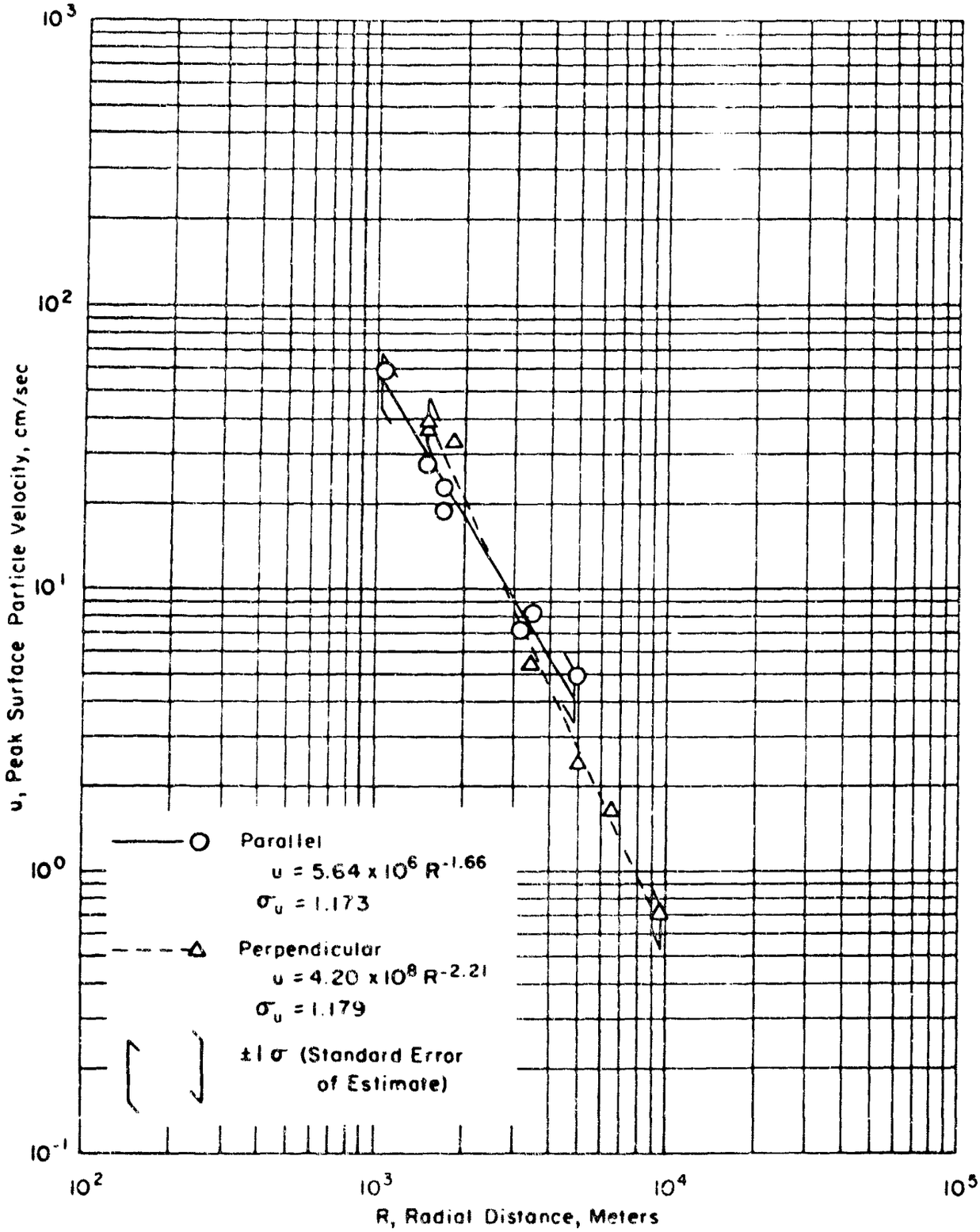

Figure 3.15 Comparison of Resultant Vector of Velocity Measured Parallel and Perpendicular to Major Fault Trend

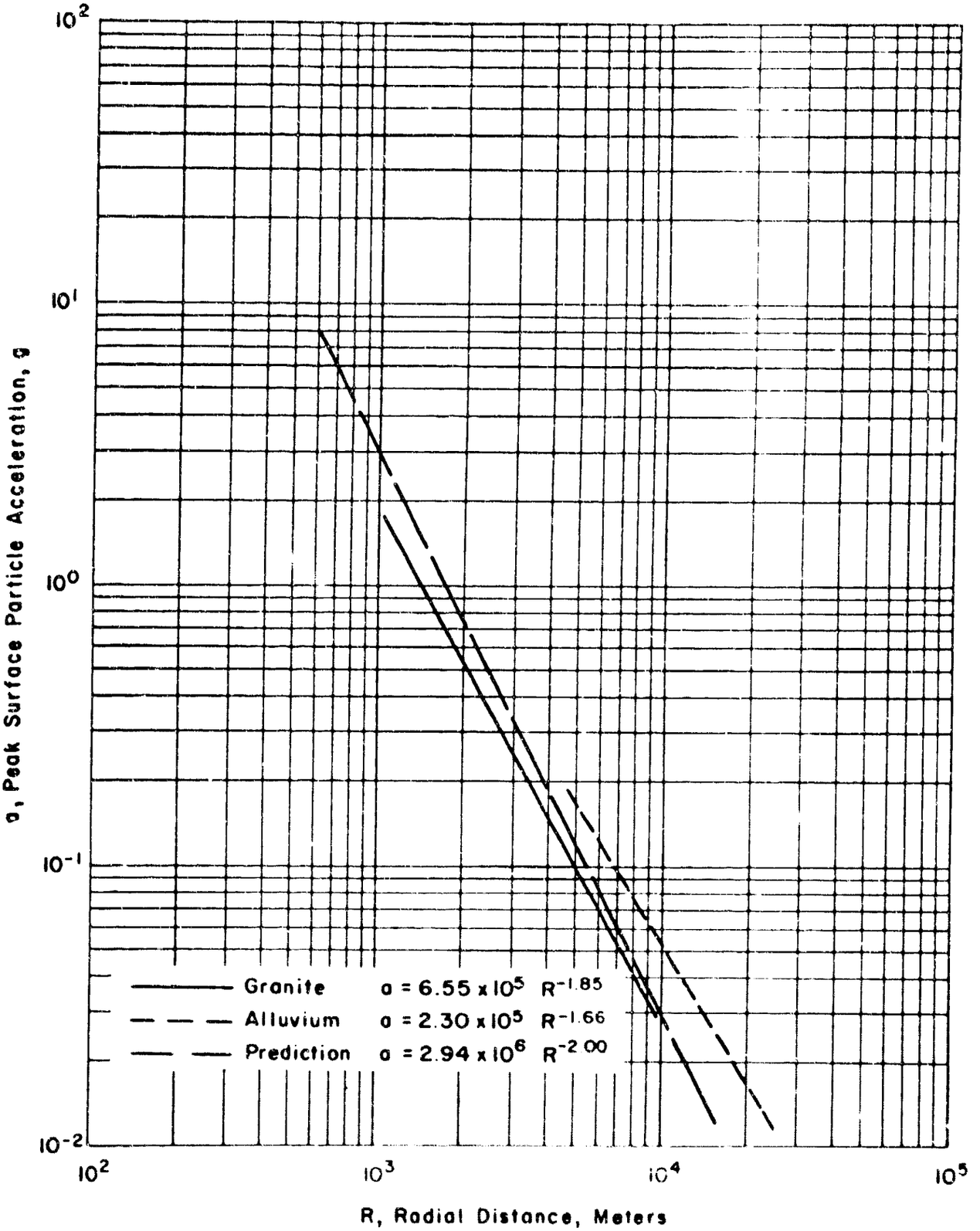

Figure 3.16 Comparison of Predicted and Observed Resultant Vector of Acceleration

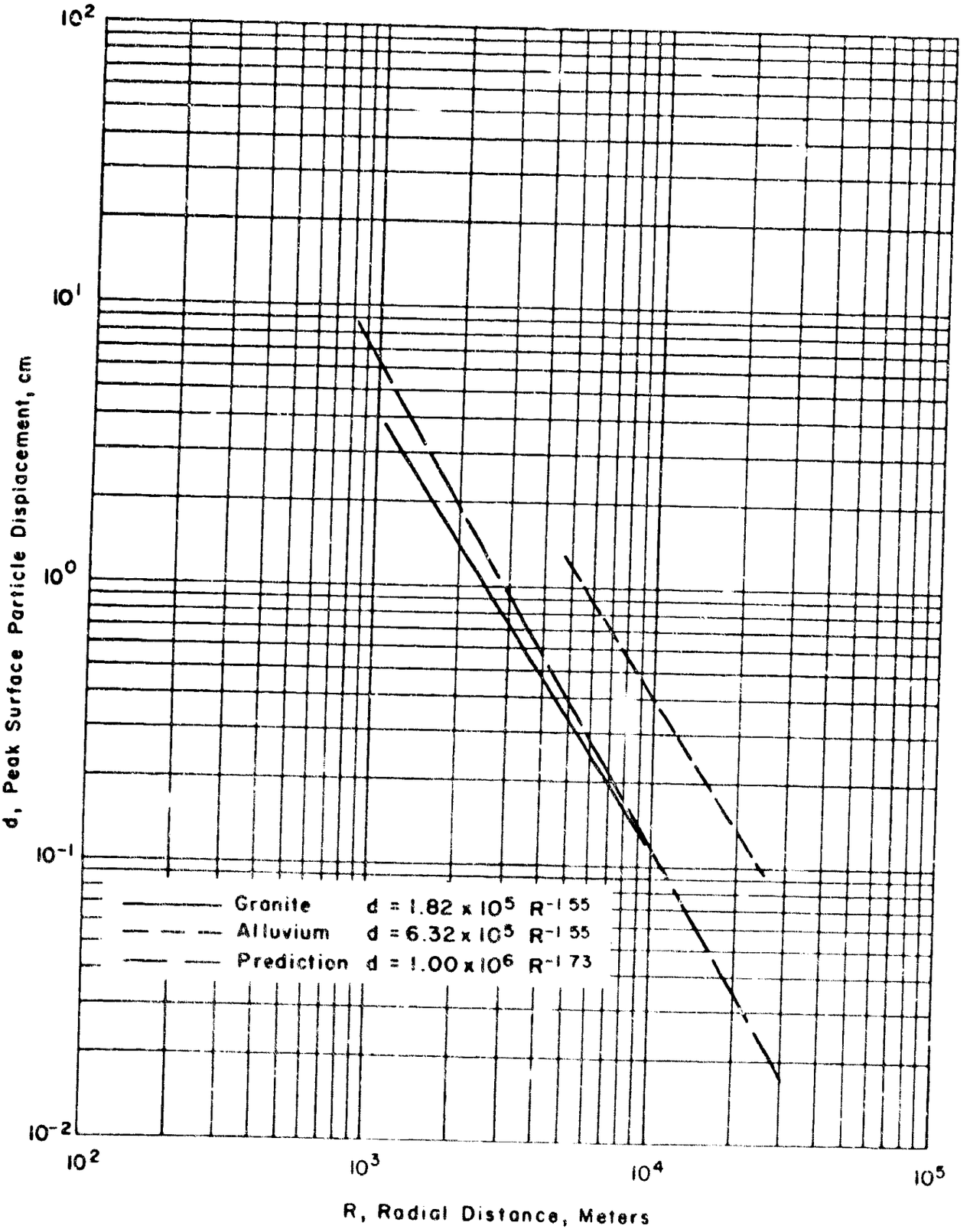

Figure 3.17 Comparison of Predicted and Observed Resultant Vector of Displacement

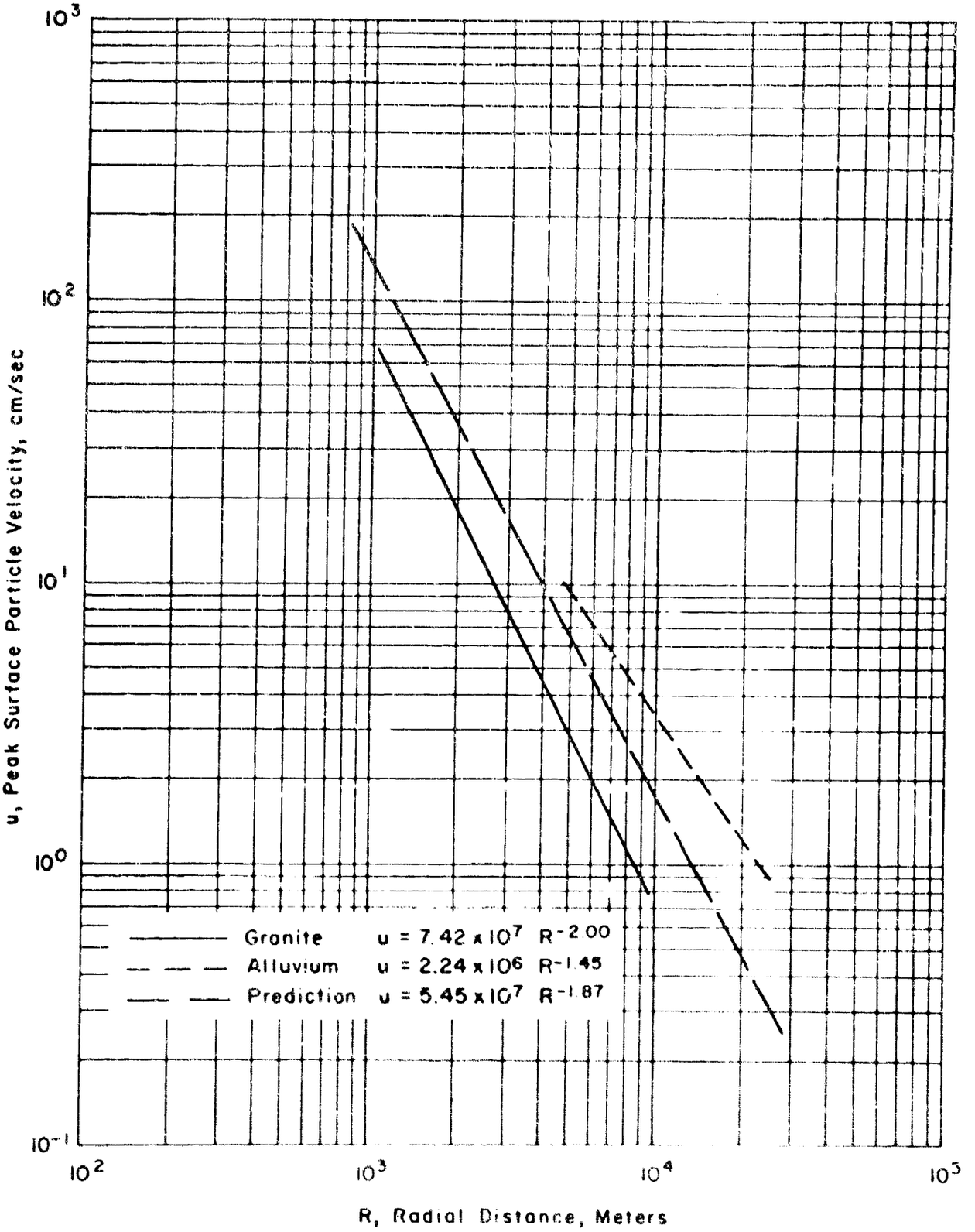

Figure 3.18 Comparison of Predicted and Observed Resultant Vector of Particle Velocity

REFERENCES

(1) University of Nevada, Reno, Nevada; "Geological, Geophysical and Hyrdological Investigations of the Sand Springs Range, Fairview Valley and Fourmile Flat, Churchill County, Nevada"; 1962; Unclassified.

(2) Fenix and Scisson, Inc., Tulsa, Oklahoma; "Drift Geology Map"; Drawing Number SHO-105-E2; 3 August 1963; Unclassified.

(3) Memorandum; Roland F. Beers, Inc., Alexandria, Virginia, from Fenix and Scisson, Las Vegas, Nevada; "Transmittal of Beers, Inc. Hole General Logs B-2, B-3 and B-4"; 10 September 1963; Unclassified.

(4) Memorandum; T. Toren to J. E. Reeves; "Project Shoal - Weekly Status Report for Period August 23-30, 1963".

(5) Interoffice Memorandum; T. Toren to J. E. Reeves, Atomic Energy Commission, Las Vegas, Nevada; "Project Shoal - Weekly Status Report for Period September 27 through October 4, 1963"; Unclassified.

(6) L. B. Werner, Hazleton-Nuclear Science Corporation, Palo Alto, California; Letter to R. H. Thalgott, Atomic Energy Commission, Las Vegas, Nevada; 19 July 1963; Unclassified.

(7) D. D. Rabb, C. R. Boardman and R. D. McArthur; "Characteristic Effects of Contained Nuclear Explosions for Evaluation of Mining Applications"; UCRL 7350; May 1963; University of California, Lawrence Radiation Laboratory, Livermore, California; Unclassified.

(8) R. D. McArthur; "Geologic and Engineering Effects - The Hardhat Event"; GN-1-63; February 1963; Lawrence Radiation Laboratory, Livermore, California; Official Use Only.

(9) J. M. Polatty, U. S. Army, Corps of Engineers, Waterways Experiment Station, Concrete Division, Jackson, Mississippi; Letter to C. F. Casey, Roland F. Beers, Inc., Alexandria, Virginia, Subject: "Project Shoal, Progress Report - Physical Properties on Granite Cores"; 1 February 1963; Unclassified.

(10) B. E. Blair; "Physical Properties of Mine Rock, Part IV including Indexes to Parts I, II, III and IV"; USBM RI 5244; August 1956; U. S. Department of the Interior, Bureau of Mines, Washington, D. C.; Unclassified.

(11) W. H. Diment, et al; "Geologic Effects of the Rainier Underground Nuclear Explosion"; TEI-355; January 1959; U. S. Department of the Interior, Geological Survey, Washington, D. C.; Unclassified.

(12) G. W. Johnson, G. H. Higgins and C. E. Violet; "Underground Nuclear Detonations"; UCRL 5626; July 1959; University of California, Lawrence Radiation Laboratory, Livermore, California; Unclassified.

(13) Roland F. Beers, Inc. Report, "Acceptability of Shoal Site from Viewpoint of Operational Safety"; 9 November 1962; Unclassified.

(14) L. M. Swift; "Measurement of Close-In Earth Motion - Hardhat Event, Nougat Series, Vela-Uniform, Preliminary Report Project 1.2"; VUP 2101; March 1962; Stanford Research Institute, Menlo Park, California; Unclassified.

(15) William R. Perret; "Free-Field Ground Motion Studies in Granite"; POR 1803; 19 April 1963; Sandia Corporation, Albuquerque, New Mexico; Official Use Only.

(16) Letter; O. H. Roehlk from A. J. Max; 1 February 1963; Subject: "Engineering Concept, Sandia Stemming Plan, Project 45.53, Shoal; Unclassified.

(17) John A. Korver, Charles R. Boardman and Donald E. Rawson; "The Shoal Post Shot Environment"; 4 February 1964; LRL Report UPOKA64-7.

(18) F. J. Turner and J. Verhoogen; "Igneous and Metamorphic Petrology"; 1951, McGraw-Hill, New York, New York; Unclassified.

(19) G. C. Kennedy and G. H. Higgins; "Temperatures and Pressures Associated with the Cavity Produced by the Rainier Event"; UCRL 5281; July 1958; University of California, Lawrence Radiation Laboratory, Livermore, California; Unclassified.

(20) W. M. Adams, et al; "Summary Report of Strong Motion Measurements, Underground Nuclear Detonations"; Project 26.0, Operation Hardtack; ITR-1711; January 1960; Unclassified.

(21) Private Communication with T. H. Pearce, U. S. Coast and Geodetic Survey, Mercury, Nevada by L. B. Luhrs, Roland F. Beers, Inc., Alexandria, Virginia; 22 October 1963; Unclassified.

(22) D. S. Carder, et al; "Surface Motions from Underground Explosions"; Phase 2, Operation Hardtack; WT-1741; March 1961; Unclassified.

(23) W. Weart, Sandia Corporation, Albuquerque, New Mexico; Verbal Communication to Sherwood B. Smith, Roland F. Beers, Inc., Alexandria, Virginia; 20 August 1964.

(24) "Project Shoal Preliminary Scientific Report"; December 1963; Sandia Corporation, Albuquerque, New Mexico; CONFIDENTIAL/DI.

(25) Roland F. Beers, Inc. Report, "Analysis of Surface Motion on Yucca Flat Alluvium for 28 Underground Nuclear Events (Addendum)"; 13 March 1964; Classified.

(26) Interoffice Memorandum; D. H. Christensen to G. H. Higgins, Lawrence Radiation Laboratory, Livermore, California; Subject: "Preliminary Report on Geophysical Logging, Pre-Shot, Project Shoal, Instrument Hole ECH-D"; 11 June 1963; Unclassified.

(27) Private Communication by R. H. Berry with Various Personnel of U. S. Geophysical Laboratories, Washington, D. C.; 1963; Unclassified.

(28) Interoffice Memorandum; R. H. Berry to R. F. Beers, Roland F. Beers, Inc., Alexandria, Virginia; Subject: "Strain at Rupture Point for Shoal Granite", 10 October 1963; Unclassified.

(29) G. A. Izett; "Granite Exploration Hole, Area 15, Nevada Test Site, Nye County, Nevada"; TEM-836C; January 1960; U. S. Geological Survey, Denver, Colorado; Unclassified.

(30) F. N. Houser; " Some Physical Property Data of Samples from U15a Site, Nevada Test Site, Table 2"; Technical Letter Area 15-2; 12 January 1962; U. S. Geological Survey, Washington, D. C.; Unclassified.

(31) F. N. Houser; "Some Physical Property Data of Samples from U15a Site, Nevada Test Site, Table 1"; Technical Letter Area 15-2; 12 January 1962; U. S. Geological Survey, Washington, D. C.; Unclassified.

(32) J. E. McDonald, U. S. Army Engineers Waterways Experiment Station, Corps of Engineers, Vicksburg, Mississippi; "Operation Nougat, Shot Hardhat, Project Officers Report, Project 9.1, Grouting Support"; POR-1807 (WT-1807); 12 April 1963; Official Use Only.

TECHNICAL REPORTS SCHEDULED FOR ISSUANCE BY AGENCIES PARTICIPATING IN PROJECT SHOAL

AEC REPORTS

Agency	Report No.	Project No.	Subject or Title
NBM	VUF-1001	33.2	Geological, Geophysical and Hydrological Investigations of the Sand Springs Range, Fairview Valley and Fourmile Flat, Churchill County, Nevada
SC	VUF-1002	40.5	Seismic Measurements at Sandia Stations
SC	VUF-1003	45.3	Hydrodynamic Yield Measurements
SC	VUF-1004	45.5	Device Support, Arming, Stemming and Yield Determination
SC	VUF-1005	45.6	Radiological Safety
EG&G	VUF-1006	60.4	Final Timing and Firing Report - Final Photo Report
USBM-PRC	*		Subsurface Fracturing From Shoal Nuclear Detonation
USWB	VUF-1008		Weather and Surface Radiation Prediction
USPHS	VUF-1009		Off-Site Surveillance
USBM	VUF-1010		Structural Survey of Private Mining Properties
USC&GS	VUF-1011		Seismic Safety Net
REECo	VUF-1012		On-Site Health and Safety Report

Agency	Report No.	Project No.	Subject or Title
RFB, Inc.	VUF-1013		Analysis of Shoal Data on Ground Motion and Containment
H-NSC	VUF-1014		Shoal Post-Shot Hydrologic Safety Report
H&N	VUF-1015		Pre-Shot and Post-Shot Structure Survey
H&N	VUF-1016		Test of Dribble-Type Structures
FAA	VUF-1017		Federal Aviation Agency Airspace Advisory
		DOD REPORTS	
SC	VUF-2001	1.1	Free Field Earth Motions and Spalling Measurements in Granite
SC	VUF-2002	1.2	Surface Motion Measurements Near Surface
** USC&GS	VUF-2300	1.4	Strong Motion Seismic Measurements
LPI	VUF-2600	1.6	In-Situ Stress in Granite
** STL	VUF-2400	1.7	Shock Spectrum Measurements
SRI	VUF-3001	7.5	Investigation of Visual and Photographic On-Site Techniques
SRI	VUF-3002	7.6	Local Seismic Monitoring - Vela CLOUD GAP Program

	TI	VUF-3003	7.8	Surface and Subsurface Radiation Studies
	USGS	VUF-3004	7.9	Physical and Chemical Effects of the Shoal Event
	ITEK	VUF-3005	7.10	Airborne Spectral Reconnaissance
	BR Ltd.	VUF-3006	7.15	The Mercury Method of Identification and Location of Underground Nuclear Sites
	NRDL	VUF-3007	7.16	Multi-Sensor Aerial Reconnaissance of an Underground Nuclear Detonation
	GIMRADA	VUF-3008	7.17	Stereophotogrammetric Techniques for On-Site Inspection
	ISOTOPES	VUF-3009	7.19	Detection in Surface Air of Gaseous Radionuclides from the Shoal Underground Detonation
***	USC&GS		8.1	Microearthquake Monitoring at the Shoal Site
****	GEO-TECH		8.4	Long-Range Seismic Measurements

---

* This is a Technical Report to be issued as PNE-3001 which will receive TID-4500 category UC-35 Distribution "Nuclear Explosions-Peaceful Applications"

** Project Shoal results are combined with other events, therefore, this report will not be printed or distributed by DTIE

*** Report dated March 1964 has been published and distributed by USC&GS

**** Report dated December 9, 1963, DATDC Report 92, has been published and distributed by UED

LIST OF ABBREVIATIONS FOR TECHNICAL AGENCIES

BR Ltd.	Barringer Research Limited Rexdale, Ontario, Canada
EG&G	Edgerton, Germeshausen & Grier, Inc. Boston, Massachusetts Las Vegas, Nevada Santa Barbara, California
FAA	Federal Aviation Agency Los Angeles, California
GEO-TECH	Geo Technical Corporation Garland, Texas
GIMRADA	U. S. Army Geodesy, Intelligence and Mapping Research and Development Agency Fort Belvoir, Virginia
H-NSC	Hazleton-Nuclear Science Corporation Palo Alto, California
H&N, Inc.	Holmes & Narver, Inc. Los Angeles, California Las Vegas, Nevada
ISOTOPES	Isotopes, Inc. Westwood, New Jersey
ITEK	ITEK Corporation Palo Alto, California
LPI	Lucius Pitkin, Inc. New York, New York
NBM	Nevada Bureau of Mines University of Nevada, Reno, Nevada
NRDL	U. S. Naval Radiological Defense Laboratory San Francisco, California
REECo	Reynolds Electrical & Engineering Co., Inc. Las Vegas, Nevada
SC	Sandia Corporation Albuquerque, New Mexico
SRI	Stanford Research Institute Menlo Park, California

RFB, Inc.	R. F. Beers, Inc. Alexandria, Va.
STL	Space Technology Laboratories, Inc. Redondo Beach Park, California
TI	Texas Instruments, Inc. Dallas, Texas
USBM	U. S. Bureau of Mines Washington, 25, D. C.
USBM-PRC	U. S. Bureau of Mines Bartlesville Petroleum Research Center Bartlesville, Oklahoma
USC&GS	U. S. Coast and Geodetic Survey Las Vegas, Nevada
USGS	U. S. Geologic Survey Denver, Colorado
USPHS	U. S. Public Health Service Las Vegas, Nevada
USWB	U. S. Weather Bureau Las Vegas, Nevada